Tomas Bata University in Zlín
Faculty of Technology

Doctoral thesis summary

Preparation and characterization of functional fillers with photocatalytic activity

Příprava a charakterizace funkčních plniv s fotokatalytickou aktivitou

Author: **Ing. Milan Masař, Ph.D.**

Study programme: P 2808 Chemistry and Materials Technology

Study course: 2808V006 Technology of Macromolecular Compounds

Supervisor: Assoc. Prof. Ing. et Ing. Ivo Kuřitka, Ph.D. et Ph.D.

External examiners: Assoc. Prof. Ing. Jarmila Vilčáková, Ph.D.

Prof. Ing. Jaromír Havlica, DrSc.

Prof. Ing. Mohamed Bakar, PhD

Zlín, December 2019

Klíčová slova: *fotokatalýza; ZnO; viditelné světlo; hybridní; stříbro; nano; C₃N₄*

Keywords: *photocatalysis; ZnO; visible light; hybrid; silver; nano; C₃N₄*

Full text of the scientific publication is available in the Library of TBU in Zlín.

Acknowledgment

Abstrakt:

Fotokatalytický jev na bázi polovodičů je v posledních dekádách podrobně studován s ohledem na velké množství aplikací jako jsou produkce vodíku, nebo čištění vody a ovzduší. V praxi jsou nejpoužívanější fotokatalyzátory, které mají široký pás zakázaných energií (band gap) a jsou fotokotalyticky aktivní pouze pod UV zářením. Aby se efektivněji využilo viditelné spektrum slunečního záření, jsou zkoumány nové fotokatalyticky aktivní polovodiče, respektive je věnována velká pozornost modifikaci stávajících. První část předložené práce je věnována teoretickému studiu dané problematiky. Na základě teoretického studia a možností realizace na Centru polymerních systémů ve skupině Multifunkčních materiálů byly stanoveny cíle předkládané práce. Byly připraveny a charakterizovány základní fotokatalyzátory na bázi ZnO. Tyto pak byly dále modifikovány nativními kyslíkovými vakancemi za účelem zvýšení efektivity fotokatalyzátoru v oblasti viditelného světla. Za účelem všeobecného zlepšení efektivity fotokatalýzy byla úspěšně prozkoumána možnost dekorace těchto základních ZnO materiálů nanočásticemi stříbra. V poslední části byla studována možnost přípravy makromolekulárního fotokatalyzátoru (grafitického nitridu uhlíku). Souběžně s přípravou fotokatalyzátorů byl vyvinut online systém pro snadnější studování jejich fotokatalytické aktivity.

Abstract:

Semiconductor photocatalysis has been studied in detail for a large variety of applications, such as water splitting or water and air treatment in the last decades. The most used photocatalysts are wide bandgap semiconductors, which are effective only under UV irradiation. In order to efficiently utilize visible solar radiation, various types of visible-light active photocatalysts are investigated. In the first part of this thesis, a literature survey on this topic is presented. According to the state-of-the-art description and current experience at the Centre of Polymer Systems in the research group of Multifunctional Nanomaterials, the Aim, goals, and objectives of the work were defined. Various types of ZnO photocatalysts were synthesized as a material base and characterized using by properly chosen analytical techniques. Later, these prepared photocatalysts were doped by native oxygen vacancies, and the effectivity of photocatalytic reaction was shifted to the visible light region. In the third part of this thesis, decoration of photocatalysts by silver nanoparticles was examined and shown to be an effective way of increasing the overall efficiency of the photocatalytic process. Lastly, macromolecular photocatalyst (graphitic carbon nitride) was investigated, and its photocatalytic activity was studied. Simultaneously, an online system for measuring of the photocatalytic activity has been developed following the current ISO norms.

Content

PREFACE

There could be no doubt that the development of photocatalysis is inspired by natural photosynthesis. G. Ciamician posed a compelling idea; to fix the solar energy through suitable photochemical reactions with new compounds that master the photochemical processes, similar to photosynthesis of the plants. The most important of these photochemical processes is the splitting of water to reactive oxygen species (ROS). Photosynthesis produces the energy necessary for life on our planet by using solar light to reorder the bonds of a water molecule to oxygen and hydrogen molecules. The hydrogen is fixed by its combination with carbon dioxide to produce carbohydrates [1]. The scale of energy stored by these chemical reactions over billions of years is far exceeding than what can be measured by known fossil fuel reserves. The recognition of this fact has inspired scientists to learn from photosynthesis and to develop technologies much more efficient and less costly than photosynthesis to meet our ever-growing energy needs.

Although early investigations in the field of photocatalysis were performed on semiconductors based on metal oxides, like ZnO and NiO, or sulfides like CdS [2,3], the short seminal note published in Nature in 1972 by Fujishima and Honda prompted a real revolution based on the extensive use of TiO_2 as a photocatalyst [4]. In this decade, interest in this semiconductor, in both academia and industry, has grown exponentially. Photocatalysis with TiO_2 photocatalyst was applied with varied success to many processes, including hydrogen production, water, and air treatment, disinfection, and organic synthesis. The relatively high quantum yield, stability over a wide range of pH, nontoxicity, low cost, and availability of TiO_2 are the critical reasons for the preponderance of this semiconductor, which has become a virtual synonym for photocatalyst [5]. Photocatalytic self-cleaning or antimicrobial coatings deposited on external building elements, like windows or roofs, along with air purifiers have already reached the mature market, and a lot of other commercial uses have been proposed, and are already on the market [6-8].

However, heterogeneous photocatalysis with TiO_2 photocatalyst has significant limitations. In general, photocatalytic reaction rates are moderate, so this technology is not appropriate for high throughput processes, such as the decontamination of heavily polluted industrial effluents. The addition of photon flux increases the reaction rate. However, saturation is achieved at relatively low irradiance. Consequently, the energetic efficiency of the process drops. However, the most crucial drawback of photocatalysis is derived from the mismatch between the TiO_2 bandgap energy and the sunlight spectra, which edge is in the UVA (400– 320 nm) and UVB (320–290 nm) ranges [9]. Mentioned technology can only take advantage of less than 6% of the solar energy impinging on the Earth's surface. Then, its potential as a sustainable technology cannot be fulfilled

entirely. This fact has deeply influenced research in photocatalysis so that modification of TiO$_2$ to achieve efficient activation by photons in the visible spectrum is a dynamic field of study [10,11].

Moreover, during the last decade, a considerable number of new photocatalysts have been synthesized and tested as an alternative to TiO$_2$, particularly in the case of solar applications, for which this standard photocatalyst is not suitable because of its wide bandgap. Instead TiO$_2$, these materials are entirely different compounds. Well-known photocatalysts like CdS or ZnO, which are historically close competitor of TiO$_2$, initially discarded because of their poor stability under irradiation, have been reconsidered for particular applications. Especially significant is the increase articles of contributions dedicated to ZnO, and it is modifications such as coupling with an additional phase (hybrid materials), doping by noble metals, or morphological changes [12].

THEORETICAL PART

1. The fundamental mechanism of photocatalytic reaction

A typical photocatalytic reaction process comprises three main steps (I-III), as shown in Figure 1. First, semiconductor photocatalyst absorbs light radiation from a light source. From the valence band (VB) of the photocatalyst are excited electrons to the conduction band (CB), while an equal number of vacant sites – holes (h$^+$) are left in the VB, forming the electron/hole pairs (process I).
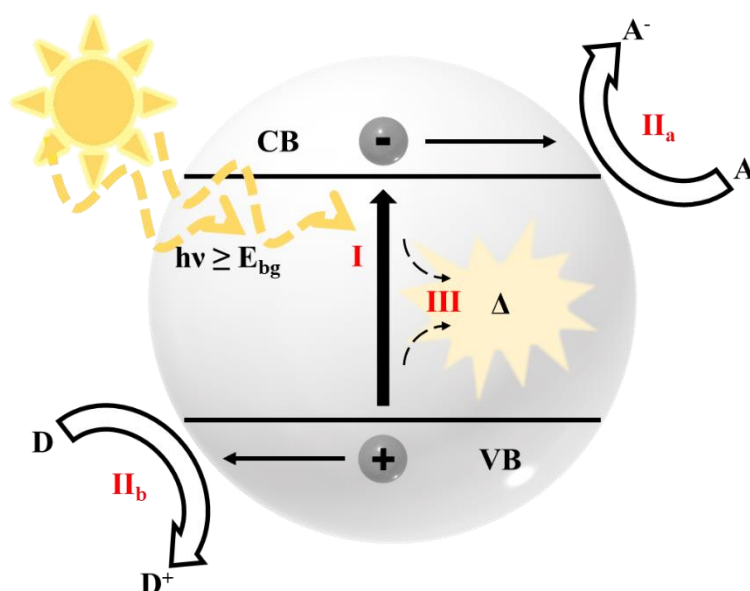
Figure 1 Schematic illustration of the basic principles of semiconductor photocatalysts. Reproduced from Ref. [13]

The energy difference between the top of the filled VB and the bottom of the empty CB is called a bandgap. Photons can excite electrons located in the VB only if their energy is greater than the bandgap width, creating thus the photoexcited state. Second, the excited electrons and holes separate in bulk and migrate to the surface of photocatalyst after photoexcitation (process II). Some of the photogenerated electrons react with an adsorbed electron acceptor, A, (process II$_a$), and holes act with an absorbed electron donor, D, (process II$_b$), respectively. The typical electron acceptor is oxygen, often provided by ambient air. The role of electron donor has water. However, there is a big chance of electron/hole pair recombination and release of energy in the form of heat or emitted light (process III). The combination of processes II$_a$ and II$_b$ is responsible for the photocatalysis. Valence band holes (h$^+_{VB}$) are powerful oxidants (typically have oxidative power of +1 to +3.5 V *vs.* NHE), whereas, conduction band electrons (e$^-_{CB}$) are reductants (usually have a reduction potential in a range of +0.5 to −1.5 V *vs.* NHE). [13].

1.1 Reactive Oxygen Species in Photocatalysis

The photocatalytic effects time-domain by the redox reactions is inflicted by photoinduced electrons (e$^-$) and holes (h$^+$) generated on the heterogeneous solid surfaces of photocatalysts. Several reactive species are generated through the reactions of molecules in the surrounding of the particles with the holes and electrons on their surface, which are considered to be involved in the actual oxidative and reductive reactions in photocatalysis as illustrated in Figure 2.

Reduction site:

$$O_2 + e^- \rightarrow {}^\bullet O_2^-$$
$${}^\bullet O_2^- - e^- \rightarrow {}^1O_2$$
$${}^\bullet O_2^- + H^+ \rightarrow HO_2^\bullet$$
$$HO_2^\bullet + e^- \rightarrow HO_2^-$$
$${}^\bullet O_2^- + e^- \rightarrow O_2^{2-}$$
$$O_2^{2-} + H^+ \rightarrow HO_2^-$$
$$HO_2^- + H^+ \rightarrow H_2O_2$$
$$HO_2^- + HO_2^- \rightarrow H_2O_2 + O_2$$
$$H_2O_2 + e^- \rightarrow OH^- + {}^\bullet OH$$

Oxidation site:

$$H_2O + h^+ \rightarrow {}^\bullet OH$$
$${}^\bullet OH + {}^\bullet OH \rightarrow H_2O_2$$
$$H_2O_2 + 2h^+ \rightarrow 2H^+ + O_2$$
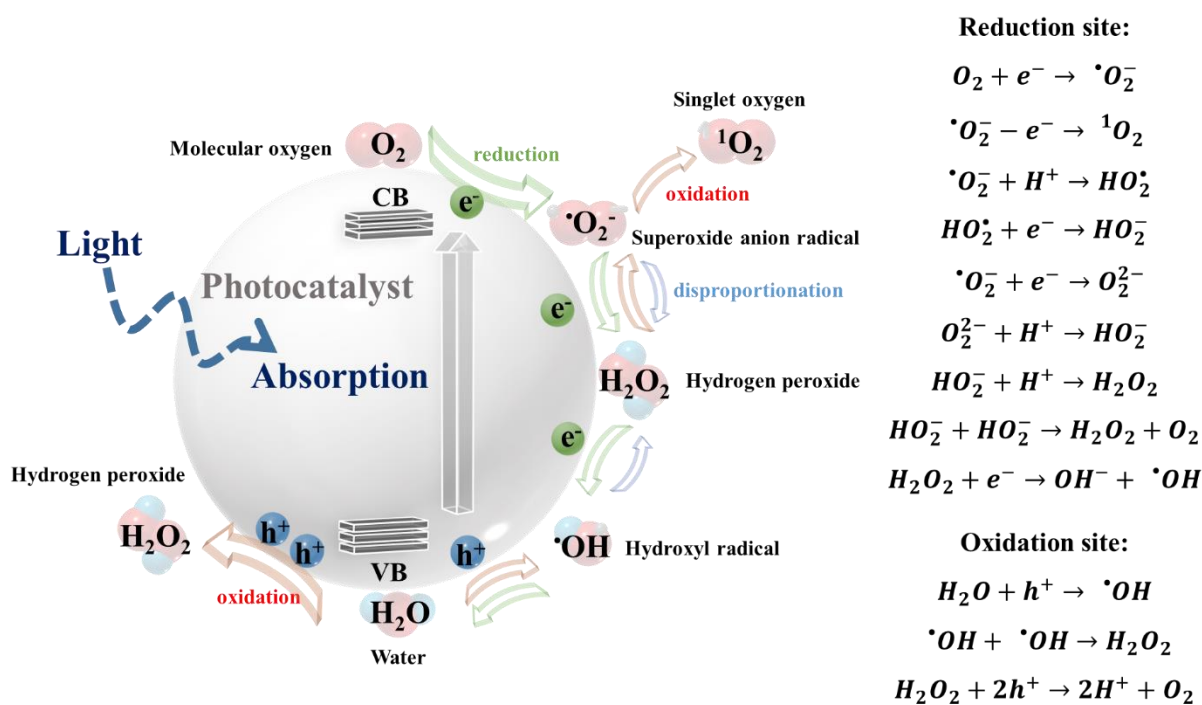
Figure 2 Reactive oxygen species generated in the photocatalytic reduction and oxidation steps of oxygen and water. Reproduced from Ref. [14]

1.1.1 Electronic states of ROS

Molecular oxygen (O_2) is a stable molecule, which has 16 electrons. Figure 3 shows the spin of electrons of O_2 at the highest occupied molecular orbitals. Major reactive oxygen species (ROS), superoxide anion radical ($^{\bullet}O_2^-$), and hydrogen peroxide (H_2O_2) are consecutively reduced from O_2 or formed from two π^* orbitals with an electron. Singlet oxygen ($^1O_2$) has the $^1\Delta_g$ state, which has higher energy than $^3\Sigma_g^-$ state of O_2 and may be produced by oxidation of $^{\bullet}O_2^-$ or by the energy transfer from the excited state of photosynthesizers. [14]
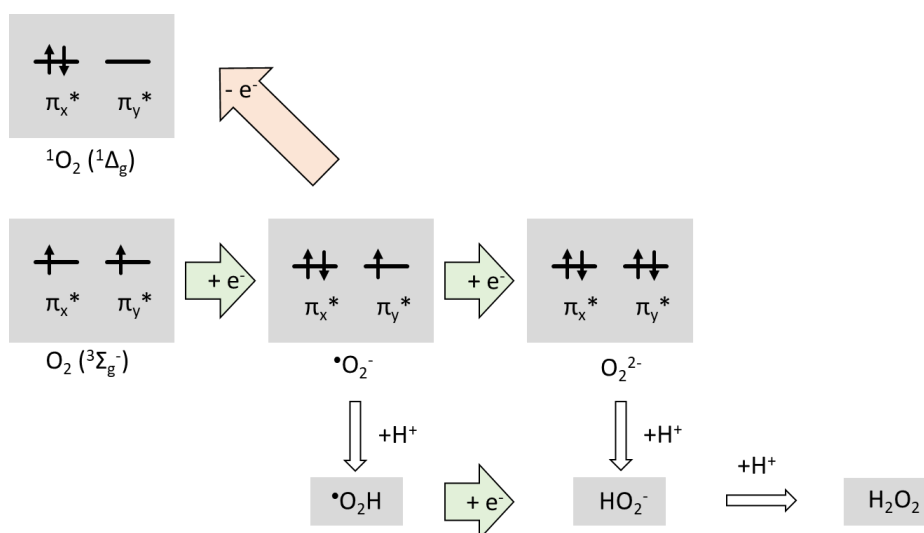
Figure 3 Molecular π^* orbitals for oxygen and ROS and their relationships [14]

Hydrogen peroxide H_2O_2 is reduced, and hydroxyl radical $^{\bullet}OH$ is formed due to O-O bond dissociation. Mentioned ROS are dependent at a pH level of aqueous solution due to the rapid acid-base equilibrium. A fundamental property of $^{\bullet}O_2^-$ is different in neutral conditions than in acidic conditions because then are protons react with that molecule, as shown in equation (1).

$$^{\bullet}O_2^- + H^+ \leftrightarrow {^{\bullet}O_2H} \quad pK_\alpha = 4.8 \tag{1}$$
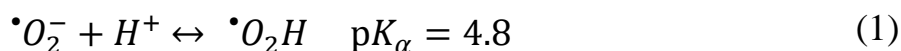
However, deprotonation of H_2O_2 and $^{\bullet}OH$ occur at a higher pH level as shown in reactions (2) and (3)

$$H_2O_2 + OH^- \leftrightarrow HO_2^- + H_2O \quad pK_\alpha = 11.7 \tag{2}$$

$$^{\bullet}OH + OH^- \leftrightarrow {^{\bullet}O^-} + H_2O \quad pK_\alpha = 11.9 \tag{3}$$
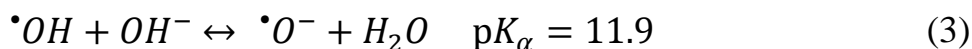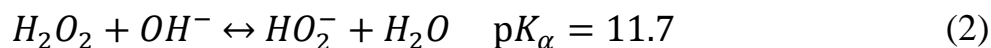
In photocatalytic reactions oxidation and reduction takes place currently. To summarize, the stepwise oxidation of H_2O leads to the generation of $^{\bullet}OH$, H_2O_2, $^{\bullet}O_2^-$, and $^1O_2$ and the stepwise reduction of O_2 to $^{\bullet}O_2^-$, H_2O_2, and $^{\bullet}OH$. [15]

1.2 Kinetics of heterogeneous photocatalysis

In a typical use, the particles of a photocatalyst are either dispersed in a liquid medium in the form of a suspension or deposited on a solid surface. The latter can be used in gas treatments as well. Photogenerated reactive charge-carriers at the surface of the particle are in contact with adsorbed molecules. Most likely, these molecules stem from the surrounding liquid suspension medium (water). It can be H_2O, OH^-, and O_2 or any gas dissolved in the liquid. Cations H^+ (H_3O^+) as well as hydroxyl anions (OH^-) are omnipresent in concentration depending on pH. The energy-rich surface states tend to perform oxidation and reduction reactions to create superoxide anion radicals $^\bullet O_2^-$ and hydroxyl radicals, $^\bullet OH$, followed by the eventual formation of other ROS [16,17]. The process continues with the reactions of these radical species with compounds dissolved in the water medium. In practice, these compounds are pollutants or contaminations, while in laboratory studies dyes are used as model molecules.

$$Pollutant + \ ^\bullet OH \ or \ O_2^{\bullet -} \rightarrow Intermediates \rightarrow Harmless \ product \qquad (24)$$
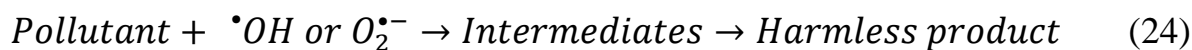
The first step of the photodegradation of organic pollutants complies with the L-H mechanism, which includes an oxidation or reduction reaction with photogenerated ROS. This step follows a quasi-first-order kinetics reaction. In a model study system, this process step is equivalent to the discoloration of the dye solution. A plethora of possible intermediate products and subsequent degradation reactions occur until the sequence of steps results into a final harmless product which is usually a pure low molecular weight compound. Ideally, the process ends up with CO_2 and H_2O formation and complete mineralization of eventual other components resulting in nitrates, sulfates, carbonates, and others. Nevertheless, the photocatalytic degradation rate r is defined in the following equation describing the first reaction step:

$$r = -\frac{dC(t)}{dt} = k_{obs}C(t) \qquad (25)$$

Where $C_{(t)}$ is the concentration of reactants at time t and k_{obs} is the rate constant.

When the concentration is shallow, the apparent rate constant r_{app} is determined from the shortened LH mechanism:

$$\ln\left(\frac{C_0}{C}\right) = k_{app}t \qquad (26)$$

Where C_0 is the concentration of the pollutant before photocatalysis; hence, the linear fit between $ln(C_0/C)$ and irradiation time determine the photocatalytic degradation rate. In model systems, the process is monitored simply by UV-Vis absorption spectrometry, and the apparent photocatalytic discoloration rate constant is estimated. Generally, the higher the k value, the better the photocatalytic activity of an examined sample is observed. [18,19]

1.3 Thermodynamics of heterogeneous photocatalysis

From a thermodynamic viewpoint, the surface reduction and oxidation reactions can be driven by the photogenerated e^- and h^+, respectively, only when their reduction and oxidation potentials lie between the CB and VB potentials. The potentials of typical reactions are shown in table 1 in Appendix I. All redox potentials given in table 1 exhibit the same linear pH dependence with a slope of -0.059 V, apart from $E^{0'}$ (O_2/O_2^-) which is pH-independent.

Photocatalytic processes are thermodynamically downhill ΔG is < 0 and are accelerated merely by the catalyst. On the other hand, photosynthetic processes are thermodynamically unfavorable; uphill ΔG is > 0 and requires photochemical energy input to occur as illustrated in Figure 4. The term ''photocatalysis'' can be applied only to the reactions occurring with a reduction in the free energy ΔG is < 0. The speed of these reactions is increased thanks to a particular reaction pathway involving unfavorable species. This pathway differs from the usual thermal reaction sequence, without irradiation, and leads to reaction product selectivity different from those for the thermal reactions.
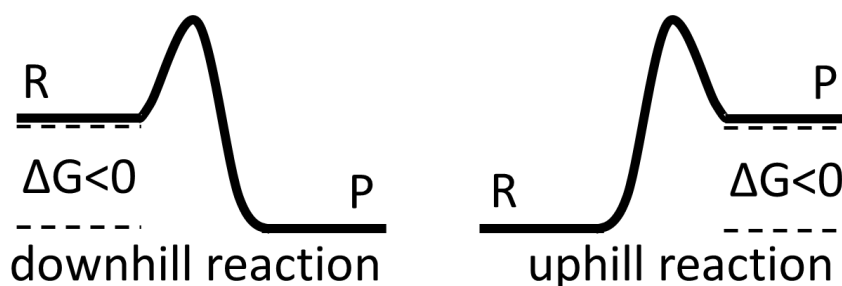
Figure 4 Thermodynamically uphill and downhill processes

For thermodynamically unfavorable reactions ΔG is > 0, the energy of UV irradiation is converted into chemical energy, and the term ''photosynthesis'' (with or without catalytic steps) applies. These two processes, photocatalysis and photosynthesis, are entirely different and should not be confused.

1.4 Application potential of photocatalytic reactions

The number of commercial products based on oxidative photocatalysis, with oxygen as the electron acceptor, is now an exciting field. Primary applications are divided into these groups: (1) water purification systems; (2) air purification materials (for example coated concrete, tiles or air-purifiers); (3) self-cleaning, building materials (paint, coated glass, concrete, pipes, and fabrics); (4) antifogging glass (coated mirrors); and (5) antimicrobial coatings (paints or sprays) [13]. The level of development of solar photocatalytic technology varies depending on the field of application and ranges from basic research to mature market-ready processes [8].

1.5 Modification strategies for enhanced or shifted (to visible light region) photocatalytic activity

Due to the wide bandgap of ZnO or TiO$_2$, UV light is commonly used as the photoinitiation source. Because solar spectrum reproduces, only 4% of UV light have applications of these semiconductors limitation. Different strategies have been presented to improve the photocatalytic activity of ZnO under the visible light – a significant fraction of the solar spectrum. Enhanced or shifted photocatalytic activity can be achieved by the following approaches, e.g., surface modification via dye sensitization, organic compound sensitization, polymer sensitization, coupling with a narrow bandgap semiconductor and bandgap engineering with the creation of defect states as well as metal and non-metal doping. [20]

1.5.1 Surface modification via noble-metal nanoparticles

Ag and Au's nanoparticles have strong absorption in the visible light region due to the plasmon resonance of e$^+$. This absorption stems from the collective oscillation of the conduction electrons under perturbation of the external electromagnetic field of the radiation. [21] The role of noble-metal nanoparticles decorated on a semiconductor surface is twofold, injected electrons by the semiconductor are easily trapped by noble metals, and they are an excellent catalyst for the reduction of O$_2$, because of they can adsorb energy from visible light. The surface e$^+$ of noble-metal nanoparticles can be promptly scavenged by O$_2$, thus avoiding the accumulation of e$^+$ on noble-metal nanoparticles and also increasing the formation of ${}^\bullet$O$_2^-$.

1.5.2 Oxygen vacancies

In comparison with other doping methods, oxygen vacancies are a kind of self-doping without the need for the addition of any elements. The intrinsic crystal structures are preserved; however, the photocatalytic activity is enhanced under the visible part of solar light. [22] Guo et al. studied the optimal concentration of oxygen vacancies, compare the low and high amount of oxygen vacancies, and established optimal concentration for ZnO [23]. The effect of oxygen vacancies on photocatalytic activity can be dependent on their position. Surface oxygen vacancies can result in lower surface recombination and participate both as charge carrier traps and as adsorption sites. While oxygen vacancies in bulk participate as charge carrier traps and sites for recombination of photogenerated carriers. In contrast to other methods for enhancement of photocatalytic performance, the native defects can be affected by post-growth treatments. Annealing of precursors is one of the most generally used methods for obtaining oxygen-rich semiconductors. [24]

1.6 Macromolecular photocatalysts

As an alternative, organic semiconductors report advantages of structural diversity, synthetic modularity, and feasibility for precise tuning of properties [25,26]. They display a marked diversity, encompassing from aromatic to heteroaromatic rings, porphyrins, fullerenes, perylene tetracarboxylic diimide, polypyridyl complexes, or phthalocyanines [27]. For a systematic treatment, photocatalysts have been grouped into the following families: pyrylium salts, aromatics, heteroaromatics, chlorins, porphyrins, and phthalocyanines. Photooxidation of pollutants using organic photocatalysts rarely leads to complete mineralization or to total elimination. Instead, highly oxidized fragmented compounds may be obtained, which are less toxic and more suitable for subsequent biological treatment.

On the border between the organic, polymer, and inorganic materials, recent literature reports on photocatalytic activity of carbon nitride (C_3N_4). C_3N_4 exists in several allotropes, namely, α-C_3N_4, β-C_3N_4, graphitic-C_3N_4 (g-C_3N_4), and cubic-C_3N_4, with various properties. The g-C_3N_4 conjugated polymer is the most stable under ambient conditions with bandgap energy ~ 2.7 eV [28]. The structure of this material resembles the structure of graphite strongly. As such, it offers similar variability of properties and possibilities of application, including the preparation of single molecular sheet graphene analogs [29]. Among other applications, g-C_3N_4 was shown to have a photocatalytic activity which may be further tuned and primarily enhanced by morphology and structure modifications and doping [30]. Moreover, the photosynthetic effect was also reported and demonstrated on photo fixation of atmospheric nitrogen.

The development of these organic photocatalysts opens the doors for another new class of materials rising hope to be prominent in two main benefit areas. First, these materials can be prepared from soft organic, renewable sources (e.g., urea) which contribute to the sustainability of any processes using them. Next, their typical bandgap fits the solar radiation spectrum filtered by the Earth's atmosphere. The use of sunlight in photocatalysis is the second way how it might result in enhanced sustainability of their utilization. [31-33]

2. Aim and goals of Dissertation

The aim and goals of the proposed work are to develop new material systems with photocatalytic activity under UV light and extend their photocatalytic activity under the visible light region. This aim was defined according to a research target of the workplace and performed a literature review.

The aim of proposed work is conceived from general (i) understanding of fundamental relationships between material properties of photocatalysts and its performance, (ii) investigation of possibilities for extension of absorption edge of traditional UV-light active photocatalysts towards visible-light in order to harvest (capture) sunlight much more effectively, (iii) enhancement of photocatalytic activity of given photocatalysts and elucidating the role of reactive oxygen species (ROS) in the photocatalytic process occurring in studied systems, and (iv) investigation of photocatalytic performance of graphitic carbon nitride (C_3N_4) as the most studied organic macromolecular photocatalyst nowadays.

This aim may be divided into following justified goals and objectives:

(I)   Principal investigation of material properties affecting the photocatalytic performance of semiconductor photocatalysts, including crystallinity, morphology, specific surface area and/or grain size, and even contribution of morphological parameters at various hierarchical levels to photocatalytic performance (will be realized on ZnO as a member of classic photocatalysts). ZnO was chosen as the model photocatalyst.

(II)   Extending of the absorption edge of ZnO, a member of traditional UV light-responsive photocatalysts will (is intended to) be done via manipulation of native defects. ZnO_2 was identified as the appropriate precursor material which, upon thermal decomposition, yield oxygen vacancies rich ZnO with modified bandgap. Evaluation of the effect of bandgap narrowing on visible light photocatalytic activity involves the development of testing apparatus suitable for the evaluation of photocatalytic performance under visible light.

(III)   The enhancement of photocatalytic activity will be realized by noble metal deposition on hierarchical ZnO photocatalyst. It comprises the development of a robust hydrothermal synthesis route, which enables the preparation of the Ag/ZnO composite precursor in one step. The role of reactive oxygen species (ROS) by scavenger experiments in a photocatalytic process will be studied.

(IV)   Synthesis and characterization of the graphitic carbon nitride (C_3N_4) as a member of organic (metal free) macromolecular photocatalysts by existing (established) methods and implementation of microwaves for shortening synthesis time. The testing of photocatalytic activity will be faced with the phenomenon of dye adsorption.

EXPERIMENTAL PART

3. Characterization techniques

3.1 Instrumental techniques and used equipment

Prepared materials were characterized by common instrumental technique available at CPS including (listed below):

Morphologies of samples were investigated by a NovaNanoSEM 450 scanning electron microscope (The Netherland, FEI Company) with the Schottky field emission electron source operated at acceleration voltage ranging from 200 V to 30 kV. The elemental microanalysis was performed by the Octane SSD (area 30 mm2) EDX (dispersive energy X-ray) detector (AMETEC, Inc).

The detailed microscopic investigation was performed with the use of transmission electron microscopy (TEM) JEM-2100 Electron Microscope (Jeol L.t.d., Japan). AN acceleration voltage of 200 kV was used throughout all experiments.

Thermogravimetric analysis (TGA) was carried out by the thermogravimeter Q500 (TA Instruments, United States) in a suitable temperature range.

The crystallinity and phase identification of powder materials were confirmed by XRD diffractometer MiniFlex600 (Japan, RIGAKU) with Co Kα source. The size of the ZnO nanocrystallites was considered to the size of the diffracting area d_{diffr} which is accessible via Scherrer's formula using $\Delta(2\theta)$ which is full-width at half-maximum (FWHM) of the line in the XRD patterns.

The specific surface area was calculated based upon the multipoint Brunauer-Emmet-Teller analysis of nitrogen adsorption/desorption isotherms at 77 K carried out using BELSORP-mini II (Japan, MicrotracBEL)

The Raman spectra were collected by dispersive Raman microscope Nicolet DXR (Thermo Scientific, United States) with an argon laser operating on 455, 532, 633 and 780 nm and measuring in the ranges 3500-85, 3550-50, 3550-50 and 3300-50 cm^{-1}, respectively.

The study of UV–vis diffuse reflectance was performed by the UV–vis spectrometer AvaSpec 2048-2 (Avantes, The Netherlands) with the light source AvaLight-DHS-DUV equipped with an integrating sphere ($BaSO_4$ coated) and white tile $BaSO_4$ reflectance standard.

The study of the UV-vis light absorption of the solutions was performed with the aid of the UV-vis spectrometer UV-Vis Varian Cary 300 (Varian Inc., United States).

Room temperature photoluminescence (PL) emission spectra were measured for all annealed samples by the FLS 920 Fluorescence spectrometer (Edinburgh Instruments, The United Kingdom).

FT-IR spectra were collected with the aid of FT-IR spectrometer Nicolet 6700 (Thermo Scientific, United States) equipped by ATR accessory.

3.2 Photocatalytic activity measurements

Due to the application potential of semiconductor photocatalysis, the international standards organization (ISO) has begun to address the need for quantification of photocatalytic testing. Our reaction is designed in that way. Catalyst particles are mixed with a fluid (water with dye pollutant), and stirring is a try to achieved uniform light distribution within this system. The degradation of pollutants is measured by spectroscopy, and photocatalytic activity is calculated from measured data. [34]

The photocatalytic activity basic ZnO material and g-C_3N_4 were evaluated by measuring the photocatalytic discoloration of the Methyl Violet 2B (MV2B) in distilled water under the constant illumination of a 100W focused UV-lamp (Super-Light C 10 A-SH, Helling Gmbh., Germany) with the strongest emission at 365 nm. In a typical experiment, 50 mg of the ZnO porous powder sample was added into the double-wall glass beaker containing 50 mL of MV2B solution, having a concentration of 3.7 mg.L^{-1}. During the experiment, 12 samples of the solution with a volume of approximately 1mL were taken within a time range of 0 to 120 minutes. The time-dependent discoloration was monitored by measuring the absorption of the MV2B solutions at 580 nm by UV-vis spectroscopy.

The photocatalytic activities of oxygen vacancies rich ZnO and hierarchically nanostructured ZnO and ZnO/Ag were evaluated utilizing degradation (discoloration) of MV2B at the concentration of 3.5 mg.L^{-1} under UV and visible light. The original method intended for online measurement of photocatalytic activity which is advantageous over commonly used experimental set-up was proposed. It is based on the homemade cuvette holder housing equipped with LED mounted directly inside the UV-Vis spectrometer. While in a standard experimental set-up the degradation of model dye and evaluation of photocatalytic activity by UV-Vis spectrometry involves two distinctive steps, i.e. degradation reaction and UV-VIS measurements are performed separately, in the experimental design presented, cuvette holder housing equipped with LED enables online UV-VIS monitoring of photocatalytic driven degradation in the course of degradation reactions. The cuvette serves as a miniature photochemical reactor with its content being mixed continuously or in a duty cycle with a small magnetically driven stirrer bar. The whole setup is visible in Figure 5.

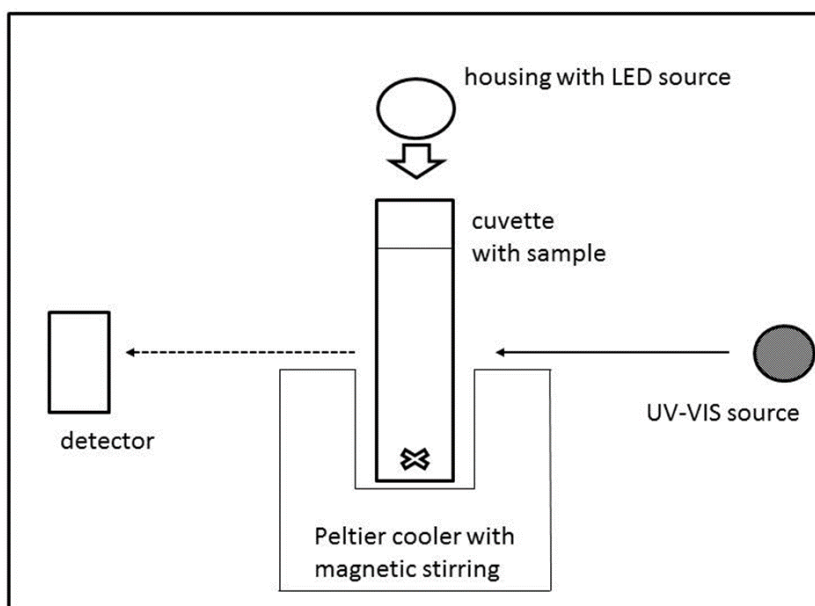*Figure 5 Schematic illustration of the photocatalytic experiment
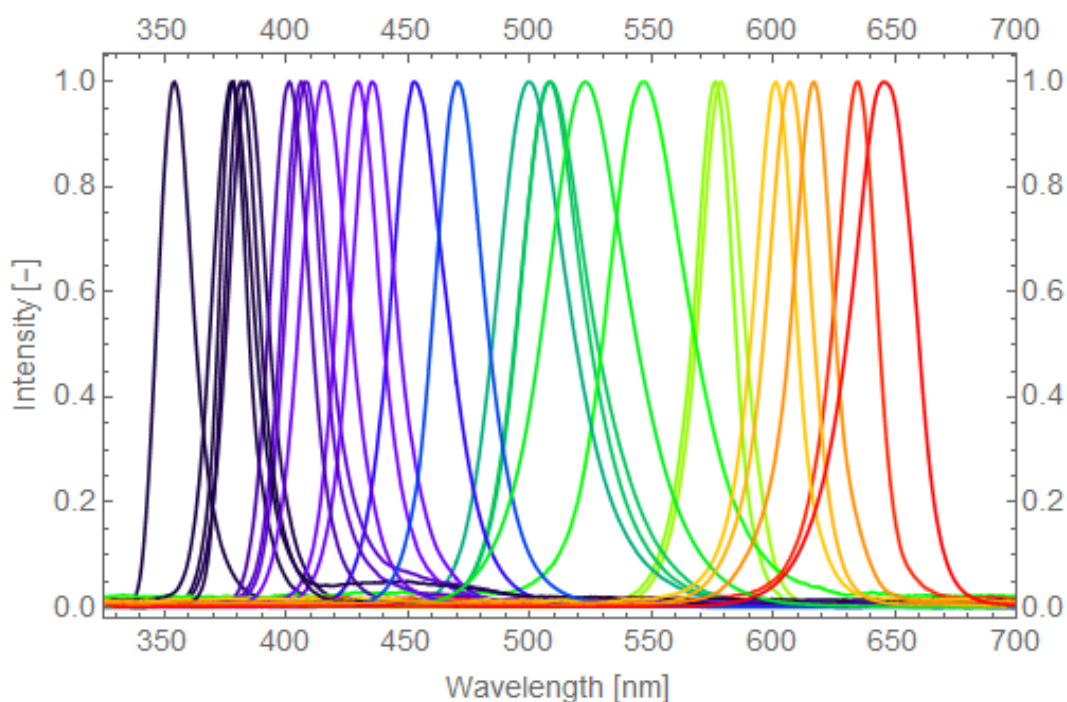performed directly inside UV-ViS spectrophotometer*

*Figure 6 Maxima wavelength of commonly available LED (Roithner
LaserTechnik, Austria)*

Moreover, LEDs can be easily changed, making an experimental set up suitable for the assessment of photocatalytic activity over a broad spectrum of wavelengths ranging from 365 to 700 nm (see Figure 6).

RESULTS AND DISCUSSION

4. Mesoporous nanostructured ZnO as a base material

The synthesis of ZnO is a topic intensively investigated in our research group for many years. It has become a standard of its kind. In the previous research [35], the formation of ZnO hierarchically structured mesoporous particles was described. These materials were prepared by annealing from a zinc oxalate dihydrate precursor at four different temperatures (400, 500, 700 and 900 °C) in an air atmosphere. Original contribution in this work was focused on the analysis of the role of reactive species in the dye discoloration process and identification of the roles of structural and morphological factors acting at different hierarchical and size scale levels of the material.

4.1 An analytical framework for the investigation of photocatalytic performance of the base material

An analytical framework for the study of contributions of morphological and structural parameters at different hierarchical morphology levels to photocatalytic activity of mesoporous nanostructured ZnO was developed. The concept of hierarchically built-up morphology at dimension scale levels is illustrated in Figure 7.
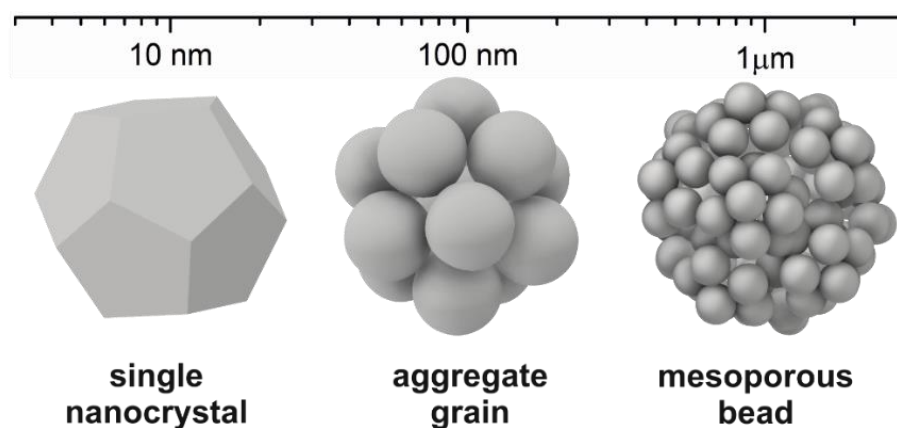
Figure 7 Illustration of morphology levels of mesoporous nanostructured ZnO microlumps

The material was prepared by annealing of an oxalate precursor and keept the overall size and the polyhedral envelope shape of the precursor on a micrometric scale. With increasing temperatures, coarsening of the particle structure can be observed. The size of the grains ranges from several tens up to several hundred nm. Sintering and coalescence of the grains was studied previously as well as changes in porosity of the materials. These observations were described in [36].

The micrometer level

First, the factors influencing photocatalytic performance of the material on the scale of the mesoporous micro-lumps size (micrometers) must be considered. Thus, their morphology including implications on the diffusion flow in their pores is examined. It is generally accepted that the catalytic activity of a heterogeneous catalyst depends on its specific surface area. However, in our case, the catalytic activity may not be correlated simply with the size of the surface area of the catalysts for at least three reasons [36]:

1. Only that portion of the surface is active which is attainable to the MV molecules by the mechanism of diffusion into the lumps followed by the diffusion of discoloration and other degradation products out of the pore labyrinth of the lumps.

2. Only that portion of the surface can contribute to the dye degradation which is closer to the lump surface than the diffusion length of the active species born on that surface such as superoxide, hydroxyl radicals, etc., if this is the mechanism.

3. The availability of the ZnO material to be irradiated by the UV, which has most likely only a limited penetration depth into the lumps.

The submicrometer level

Next lower level in the hierarchically organized morphology can be found at the size scale of hundreds of nanometers, i.e. mainly the influencing factors of the photocatalytic performance of the material emerging on scale of individual ZnO grains is investigated. At the morphology level of a single grain, the exciton diffusion length may be the critical factor controlling the photocatalytic performance. Only those excitons which come into contact with a surface exposed to the reaction medium can be involved in the reduction (electron) and the oxidation (hole) reactions. All other excitons end up in the futile electron-hole recombination. [36]

The nanoscale

Single ZnO nanocrystallites can be considered the smallest building blocks (on the size scale level of tens of nanometers) of the studied hierarchically structured material. Because of their size is in tens of nanometers, it might be reasonable to examine eventual quantum confinement effects. [36]

The molecular level

Concerning the identification of the molecular mechanism of dye molecule degradation, a study utilizing scavengers can deliver decisive information. Dye molecule can be degraded either by direct oxidation or reduction by holes or electrons, respectively. alternatively, the dye is degraded by engagement of ROS intermediates into the degradation mechanisms. [36]

4.2 Morphology levels versus photocatalytic activity of the base material

The prepared micro-beads were tested in a standard test of photocatalytic activity based on an organic dye solution discoloration. Obtained discoloration curves are plotted in the graph in Figure 8. The process followed pseudo-first order kinetics and its rate constant was evaluated [35,36]. Maximum activity was found for the material prepared by annealing at 500 °C. Therefore, the photocatalytic activity cannot be explained within a simple trend of structure property (specific surface area or nanocrystallite size) correlation since factors acting both as promoting and impeding the photocatalytic activity are manifested. [36]
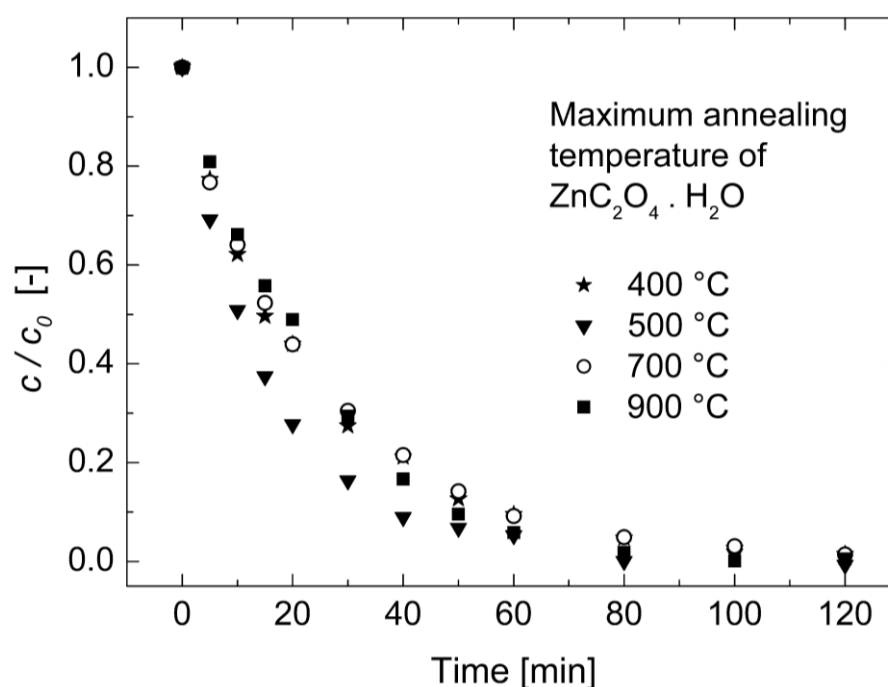

Figure 8 The photocatalytic degradation curves of the methyl violet as a function of time for the ZnO powders annealed at different temperatures [36]

4.3 Identification of photocatalytic mechanism at the molecular level

In order to complete the investigation of the photocatalytic mechanism also on the molecular level, a study employing scavengers of selected active species was performed. The results obtained for the optimum material (prepared at 500 °C) are exemplified in Figure 9. It is evident, that ethylenediaminetetraacetic acid (EDTA) as the hole scavenger kills the discoloration process, while the addition of hydroxyl radical scavenging *tert*-butanol (*t*-BuOH) slows the discoloration process only moderately. Thus, it means that a hole preferentially interacts with adsorbed dye molecule cation directly. The interaction of a hole with adsorbed

hydroxide anion to produce •OH radicals which subsequently reacts with the MV molecular cation in the solution is of lower importance. [36]
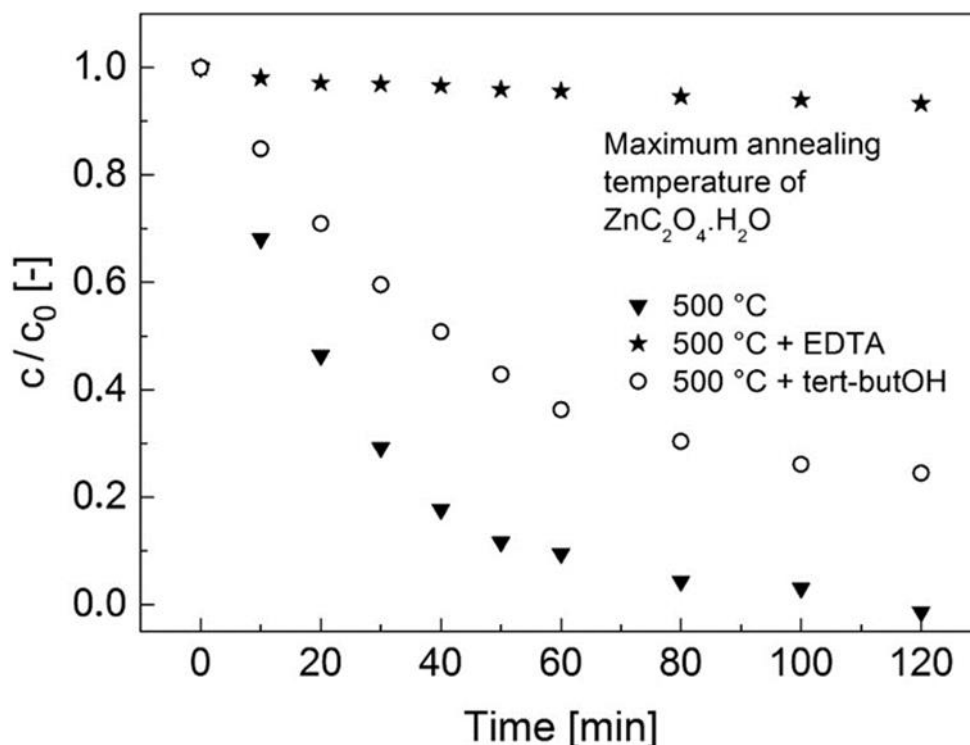

Figure 9 The photocatalytic discoloration curves of the methyl violet as a function of time for the ZnO powder annealed at 500 °C in the presence of scavengers [36]

5. Bandgap modification of ZnO

Tailoring of the bandgap of the ZnO semiconductor can be realized either by doping with atoms of other elements or by intentional manipulation of the concentration of defects that can naturally occur in the ZnO crystalline structure. The latter approach was chosen for ZnO bandgap modification in this work. The method for the preparation of raspberry-like ZnO nanocrystals assembly with tunable band gaps at a large scale is proposed. It is based on calcining of ZnO_2 precursor, which can be obtained easily at laboratory temperature via ammonia evaporation induced crystallization of the reference ZnO powder dissolved with the aid of H_2O_2. Raman, XRD and TG analysis combined with UV-Vis and PL spectroscopy revealed, that rapid release of peroxide ions during the phase transformation from cubic ZnO_2 phase to hexagonal wurtzite ZnO phase resulted in oxygen vacancies rich ZnO and that the concentration (depends on calcining temperature) of these vary with calcining temperature. The absorption edge of powders first redshift with increasing temperature up to 500 °C and then blueshift, corresponding to the gradual change in color of powder from white to pale yellow and back to white with a tinge of green.

22

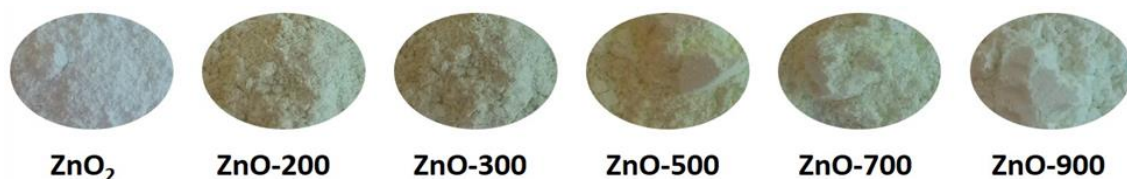## 5.1 Preparation of raspberry-like ZnO nanocrystals

Figure 10 photo images of ZnO2 precursor and products of its calcining at various temperature, including ZnO basic material system (ZnO-ref)

Precursor ZnO_2 powder was prepared by ammonia evaporation induced recrystallization of dissolved ZnO reference powder as follows; 4.2 g of ZnO was added to the 350 mL of 25-29 % aqueous solution of ammonia and stirred at 350 rpm for 10 minutes. After that, 14 mL of H_2O_2 was added, which caused ZnO to dissolved readily. The obtained clear solution was filtered to remove impurities, spread out onto Petri dishes, and left dry in the hood. The amount of solution in Petri dish 10 cm in diameter was optimized to be 20 mL. Ammonia evaporated quickly, and dry ZnO_2 precursor powder was collected after 2 hours. The precursor powder was calcined in a muffle furnace with a static air atmosphere at various temperatures alternating from 200 to 900 °C for two hours.

5.2 Characterization of raspberry-like ZnO nanocrystals

The gradual increase of samples crystallinity with increasing calcining temperature corroborate with a morphology observation, as documented in a series of scanning electron micrographs in Figure 11.
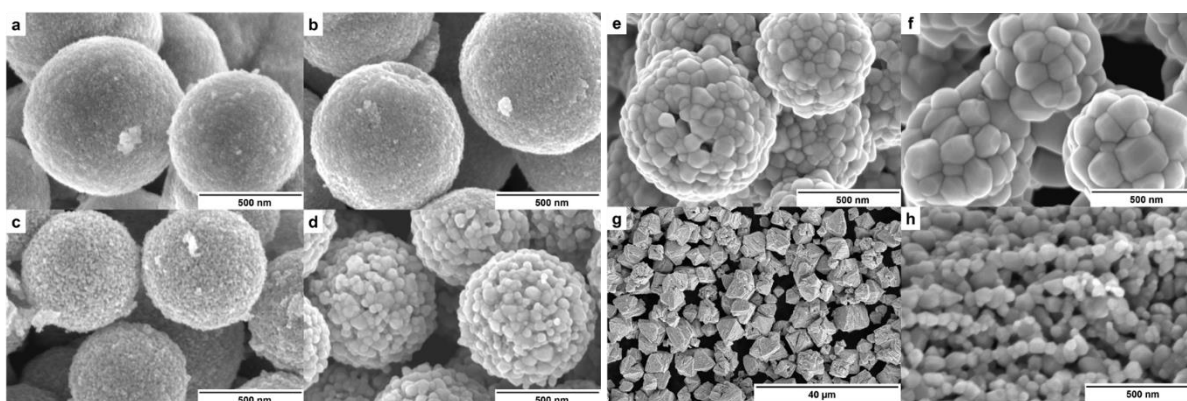

Figure 11 SEM images of ZnO2 precursor (a), and products of its calcining at various temperature; ZnO-200 (b), ZnO-300 (c), ZnO-500 (d), ZnO-700 (e) and ZnO-900 (e). Reference powder ZnO-ref at low and high resolution (g,h).

5.3 UV and Visible light activity of raspberry-like ZnO nanocrystals

The original experimental arrangement of photocatalytic experiment suitable for examination of photocatalytic activity of powder photocatalysts in the visible-light region was successfully demonstrated on a prepared sample. The LED can be easily changed with a narrow interval of wavelengths over a broad spectrum of wavelengths. With an advantage, prepared samples were evaluated in the close vicinity of estimated bandgaps by using diodes with maxima at 365 nm, 400 nm, and 425 nm. The results of discoloration studies are divided into three sets of degradation curves and shown in Figure 12, Figure 13, and Figure 14 for used wavelength 365 nm, 400 nm, and 425 nm, respectively. Reference ZnO powder exhibits a significantly higher value of the rate constant of MV2B photocatalytic degradation than oxygen vacancies rich ZnO samples under irradiation by 365 and even 400 nm diodes, while sample ZnO-500 containing samples outperformed ZnO-ref at 425 nm. However, contribution to the overall photocatalytic activity becomes negligible under irradiation by 425 nm diode.
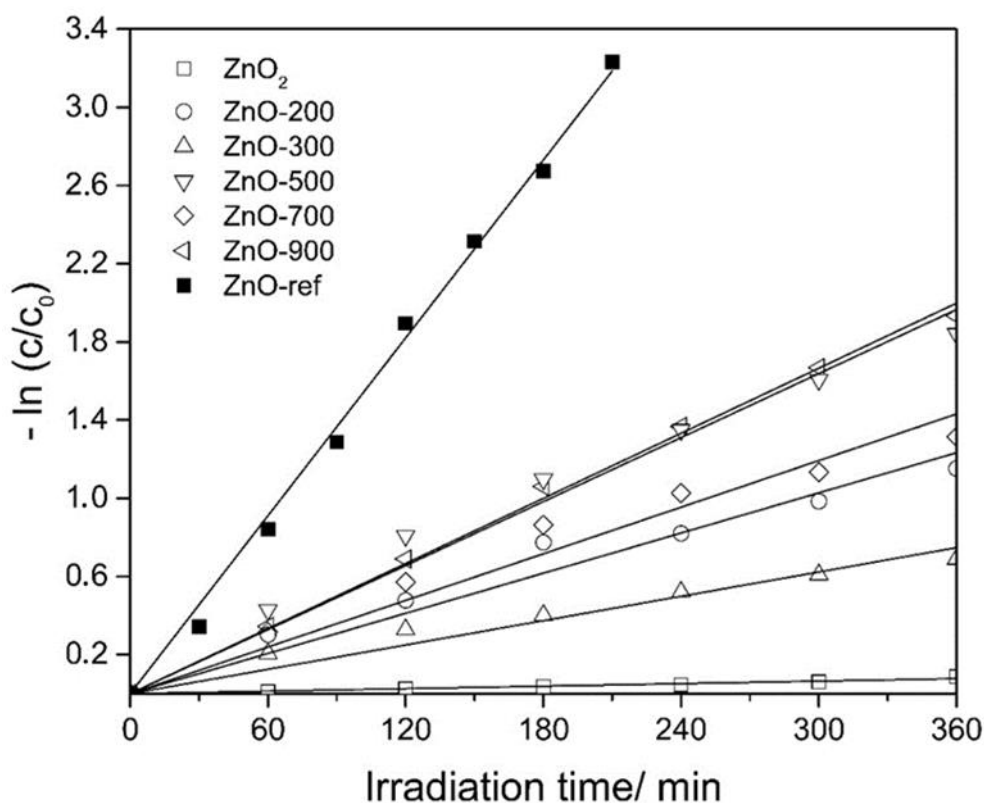

Figure 12 Photocatalytic activity of samples under the UV light irradiation (diode maxima at λ=365 nm)

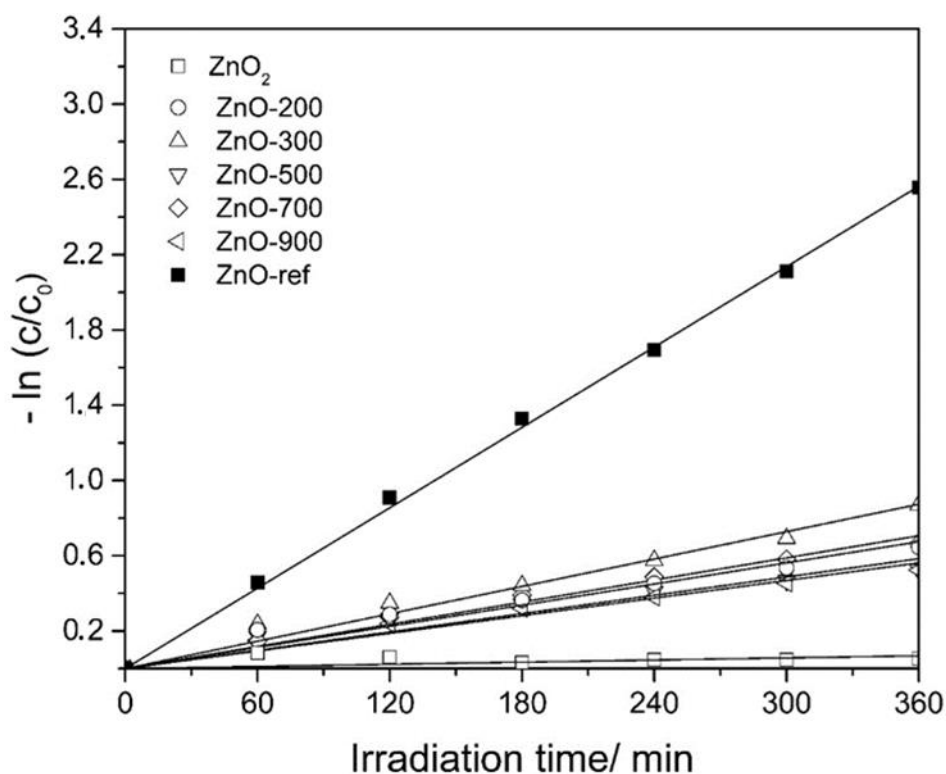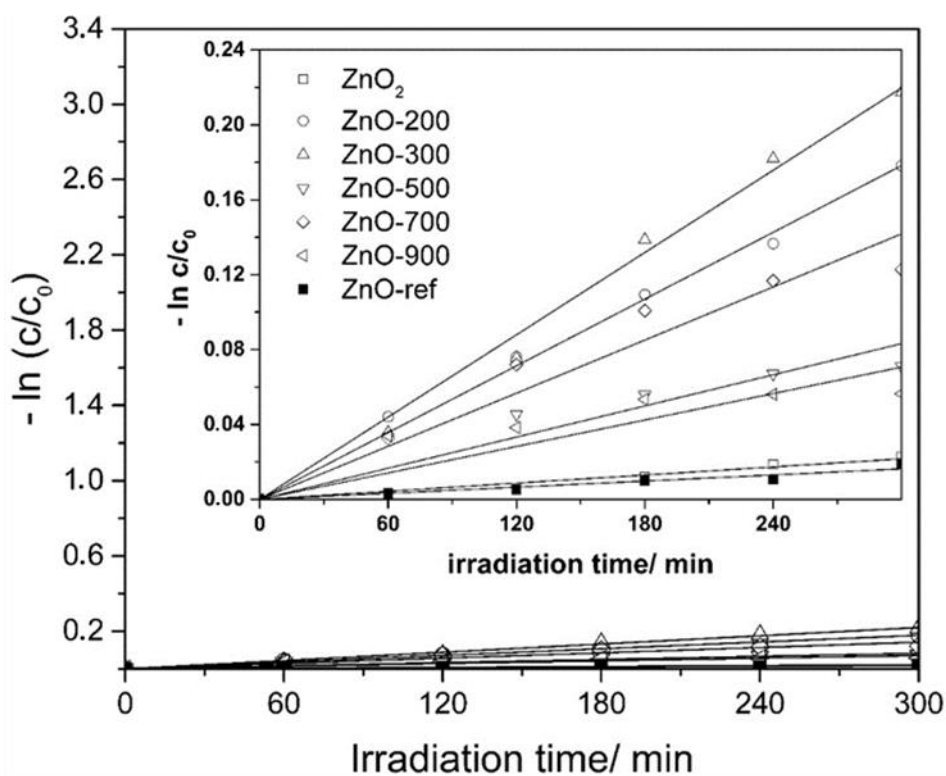*Figure 13 Photocatalytic activity of samples under the visible light irradiation (diode maxima at λ=400 nm)*

Figure 14 Photocatalytic activity of samples under the visible light irradiation (diode maxima at λ=425 nm)

6. Hierarchically nanostructured ZnO and Ag/ZnO flower-like morphologies

Hierarchically nanostructured ZnO with flower-like morphology and its Ag nanoparticles decorated Ag/ZnO analog were prepared via microwave-assisted hydrothermal synthesis of precursor material and its subsequent thermal decomposition at 500 °C. Flower-like ZnO morphology possesses significant photocatalytic activity, which can further be enhanced by the decoration of Ag nanoparticles with uniform distribution with a diameter of about 20 nm which was obtained by merely adding silver nitrate to the reaction mixture.

6.1 Preparation of 3D hierarchically nanostructured ZnO and Ag/ZnO

Synthesis of 3D hierarchically nanostructured ZnO and Ag/ZnO consists of two steps. In the first, precursors were prepared in the microwave open vessel system MWG1K-10 (RADAN, Czech Republic) operated in a continuous mode as follows; $Zn(CH_3COO)_2.2H_2O$ (10 mmol), $K_3C_6H_5O_7.H_2O$ (1 mmol) and $(CH_2)_6N_4$ (10 mmol) were dissolved in 50 mL of distilled water, respectively. Obtained solutions were mixed in a reaction bottle, placed into the microwave oven cavity and exposed to microwave irradiation. The reaction was finished after 20 minutes, and the system was left to cool down naturally. Resulted white precipitates were collected by filtration, washed with distilled water several times and dried in an oven at 70 °C. ZnO and Ag/ZnO hierarchical nanostructures were obtained by calcining of precursors at the temperature 500 °C for two hours (heating rate 10 °C/min) in a muffle furnace with a static air atmosphere. [37]

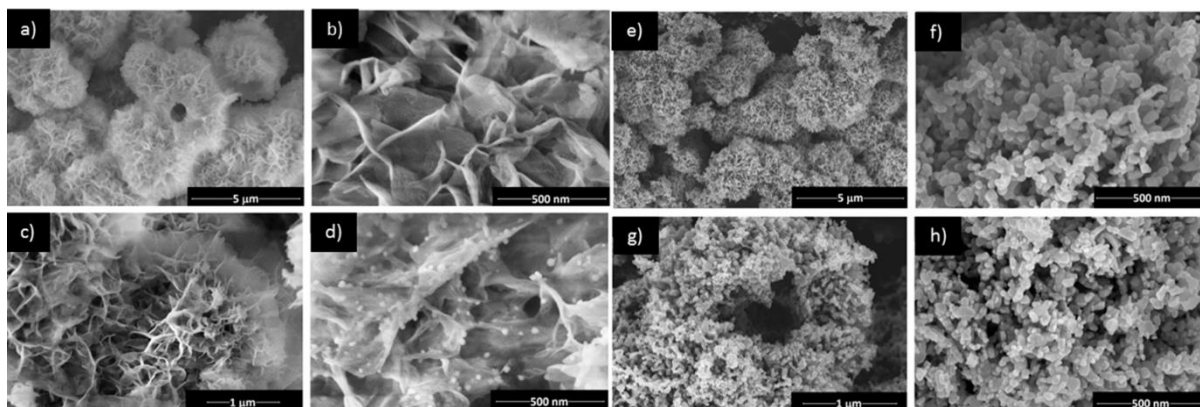## 6.2 Characterization of 3D hierarchically nanostructured ZnO and Ag/ZnO

Figure 15 Low and high-resolution SEM images of ZnO (a, b) and Ag/ZnO (c,d) precursors; ZnO (e, f) and Ag/ZnO (g, h) obtained by calcining precursor

The SEM images of hierarchical ZnO and Ag/ZnO precursors with flower-like morphologies prepared by MW assisted hydrothermal of zinc acetate, silver nitrate, tri-potassium citrate, and hexamethylenetetramine are demonstrated in Figure 15. The varying concentration of hydroxyl and citrate anions indicates precursor morphology. Citrate anions play an important role in the formation mechanism of LBZA precursor. Flower-like LBZA precursor morphology decorated with Ag nanoparticles distributed uniformly onto its surface can be easily obtained by introducing silver nitrate into the reaction mixture. Nanostructured ZnO and Ag/ZnO morphologies possess flower-like shape after calcining of precursor materials at 500 °C.

6.3 Measurement of photocatalytic activity and influence of scavengers to ROS

The plot of $-ln(c/c_o)$ versus irradiation time of all samples shows a linear trend which suggests that photocatalytic driven decomposition of dye follows pseudo-first-order kinetics, as can be seen in Figure 16. ZnO/Ag1 and ZnO/Ag2 exhibit a significantly higher value of the rate constant of MV2B photocatalytic degradation than the ZnO sample under UV irradiation, due to the metal/semiconductor heterojunction further facilitate charge carrier separation.

Figure 16 The photocatalytic discoloration curves of the MV2B as a function of time for the ZnO and ZnO/Ag

The presence of active species was studied by scavenger experiments. In which, EDTA acted as holes (h^+) scavengers, and of t-BuOH acted as hydroxyl ($^\bullet$OH) radical scavengers. The curves in Figure 17, and Figure 18 show the impact of active species on photocatalytic activity. Without the addition of scavenger, the

activity significantly increases with a decoration of Ag. The EDTA stops the photocatalytic process, and *t*-BuOH slows the discoloration process.

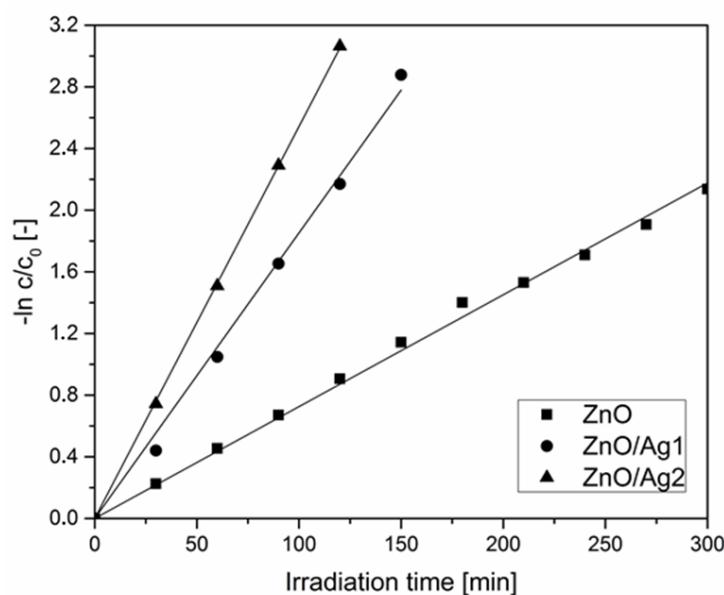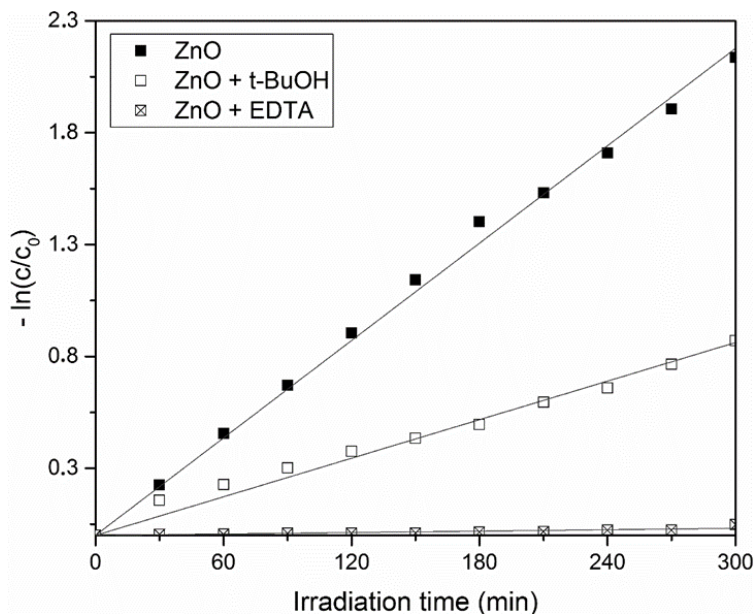*Figure 17 The photocatalytic discoloration curves of the MV2B as a function of time for the ZnO in the presence of scavengers*
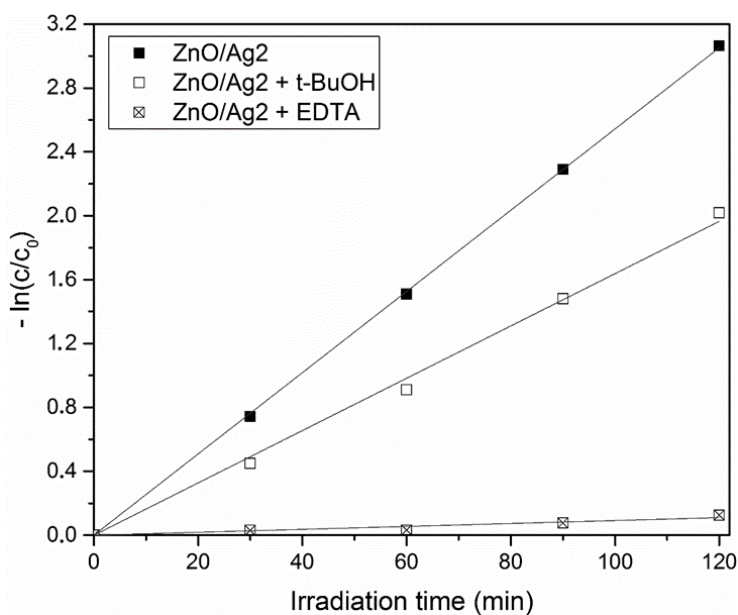

Figure 18 The photocatalytic discoloration curves of the MV2B as a function of time for the ZnO/Ag in the presence of scavengers

7. Preparation and characterization of macromolecular photocatalyst – expanded g-C₃N₄

The work on the most challenging part of the organic photocatalysts was done and is already published. Microwave-assisted heating was successfully employed in significantly accelerated preparation of expanded g-C₃N₄ via thermal condensation of urea. Comparing the typical synthesis route and rapid microwave-assisted heating enables not only shorten synthesis time from hours to a few minutes but obtain a reasonable yield of the product also. Utilization of ceramic kiln "hotpot" with an intern covered with an absorbing layer plays a crucial role in transformation of the microwave energy into heat. Heat energy in form of radiation from the glowing inner layer surface is focused on the internal volume of the kiln resulting in a swift temperature increase of a small reaction crucible containing source material load. Thus, microwave non-absorbing starting material is extremely fast heated, which results in expanded morphology analogous to that of expanded graphite. [38]

The effects of reaction conditions (i.e., time and achieve maximum temperature) on the structural, morphological, optical, and photocatalytic properties of prepared g-C₃N₄ were investigated in detail. Photoluminescence emission of the material can be continuously tuned, covering the blue to the green light region of visible light by simply changing the reaction time. The photocatalytic degradation of MV2B reveals that the adsorption capacity of samples increases with processing time while the rate constant slightly decreases. It can be ascribed to the expansion of the internal surface, which results in its worse availability to the diffusion transport of the dye to active sites. It also impedes photodegradation product removal. [38]

7.1 Synthesis of g-C₃N₄

The g-C₃N₄ was prepared by the thermal treatment of urea in a self-supporting gas atmosphere. An alumina crucible containing 5 g of urea was covered by a lid and placed into a ceramic kiln (hotpot) equipped with a microwave absorbing layer. Through this thin layer, the energy of high-frequency alternating electric field in the cavity of a standard household microwave oven (Hyundai, MWM 1417 W) was dissipated, and the internal of the kiln including the crucible and the sample was extremely fast heated. The oven was operated at 750 W for 11- 15 minutes with 1-minute steps. The final maximum temperature achieved was monitored by an infrared contactless thermometer after switching off the microwave oven. Afterward, the kiln was taken out of microwave cavity and left to cool down naturally. Samples were labeled according to the synthesis time 11-16 minutes as MW11-16, which corresponds to the final maximum temperature inside the ceramic kiln ranging from 480 to 560 °C. The temperature of absorbing

layer was much higher during operation of microwaves as a red-orange glow was observed which corresponds to a temperature above 900 °C. The yield of these syntheses was 4 to 5 % concerning the theoretical mass of the product calculated from initial source compound load assuming ideal stoichiometry. There was no observable trend of the yield dependence on synthesis time, but the sudden total decomposition experienced for times longer than 16 minutes. For comparison with a conventionally produced material, a reference sample was prepared in Muffle furnace with a heating rate of 10 °C/min and then held at a temperature of 550 ° for three hours. The reference sample is labeled as MF. The yield in this conventional technique was practically the same as in MW. [38]

7.2 Characterization of g-C_3N_4

Morphology of particles obtained by the proposed procedure and by conventional heating in the muffle furnace (high magnification images) as well as their assembly into the bigger unites (low magnification images) were investigated via SEM, and acquired images are shown in Figure 19. As can be seen, the morphology of g-C_3N_4 powder prepared in Muffle furnace (Figure 19ac) differs significantly from those made in microwaves (Figure 19d-g). While the powder obtained by conventional heating (Figure 19a) consists of small flakes with diameter around 1-2 μm, all powders obtained with assistance of microwaves are much more coarse, forming expanded aggregates with diameter of around 20 μm as demonstrated in Figure 19d,e for samples MW11 and MW16, respectively. Smaller and dense or compact aggregates observed in the MF case can be attributed to slow sintering of precursor during long time exposure to high temperature in the conventional oven, while large aggregates obtained from MW resemble expanded graphite morphology due to rapid increase of temperature. Therefore, we ascribe the expansion to the swift heating of the material and fast development of gaseous urea decomposition products, while the slow process in conventional oven did not release the gas fast enough, and there was much less or no expanding force unfolding the layered material. The high-resolution image in Figure 19c reveals that small aggregates in sample MF are formed of thin sheets entangled together. The morphology of samples obtained by microwaves has evolved with the duration of synthesis as shown in Figure 19f,g for sample MW11, and M16, respectively. The size of individual sheets increased with increasing synthesis time, which also provides rise in the maximum process temperature. The process resembles slightly unwrapping accompanied by sheet growth. There is no effect in both systems that could result in formation of thicker layer slabs, e.g. no external gas over-pressure or mechanical compressing force. However, there are no data on long time scale experiments. If the material was exposed to MW heating too long, which means longer than 16 minutes, the temperature exceeded the material's stability limit, and total decomposition was evidenced. [38]
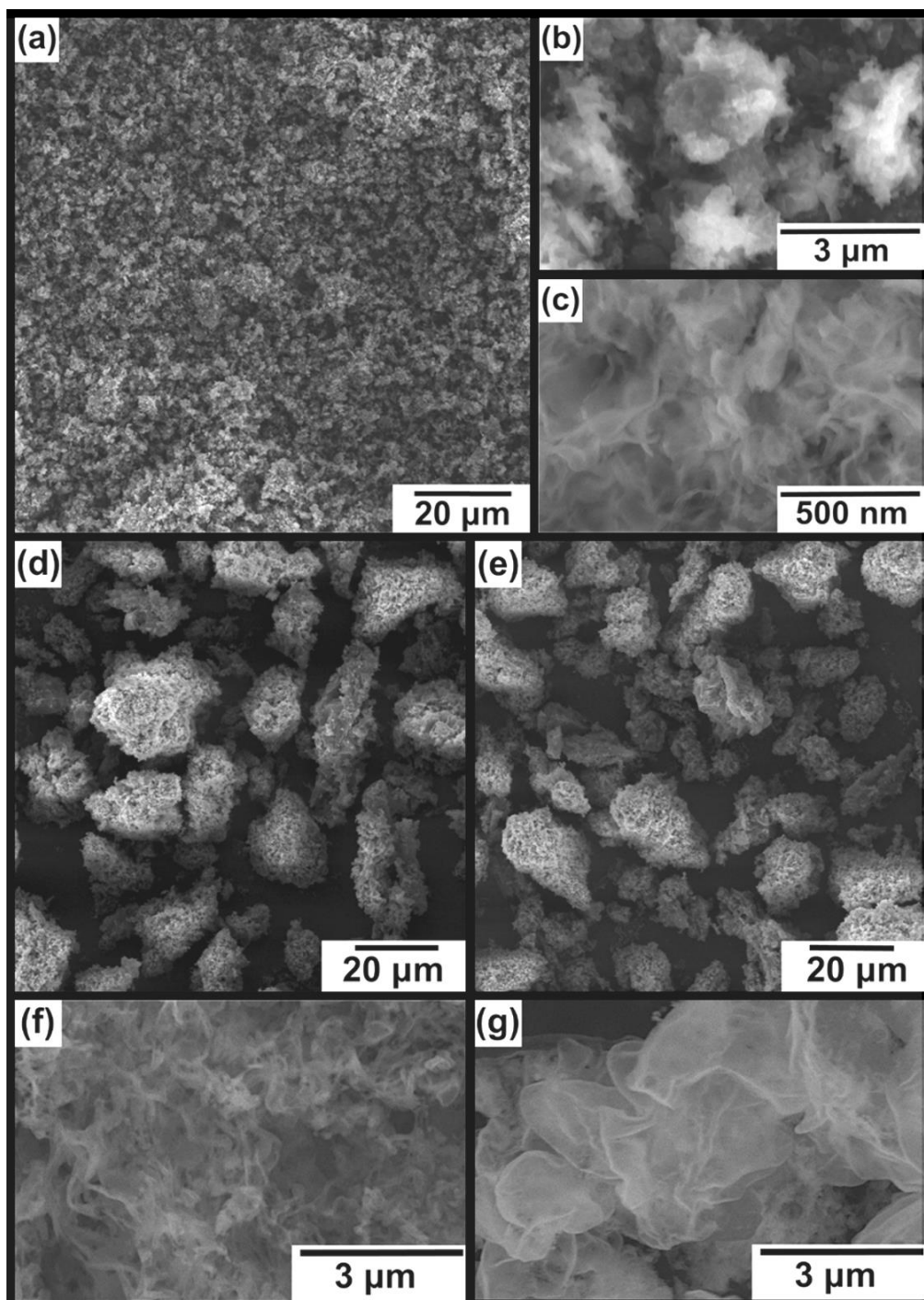
Figure 19 SEM images of samples prepared in muffle furnace MF (a-c), and microwaves with different synthesis time MW11 (d, f) and MW16 (e, g) [38]

7.3 Photocatalytic activity of prepared g-C$_3$N$_4$ organic macromolecule photocatalyst

The results on the photocatalytic degradation of MV in aqueous solution by g-C$_3$N$_4$ obtained at different reaction conditions under UV irradiation are shown in Figure 20. As mentioned above, samples were kept in the dark for one hour to

reach equilibrium conditions as a necessary prerequisite step for UV degradation experiment. Then, the samples were exposed to UV radiation, and the fading of MV solution in time was monitored by absorbance measurements in spectral resolution (see an example in the inset in Figure 20). The change of MV concentration was evaluated by the plotting normalized absorbance (i.e. $C/C0$) at the wavelength 584 nm, and rate constants were estimated from the pseudo-first-order kinetic models fitted into experimental data points in Figure 20. A set of similar curves was obtained. [38]
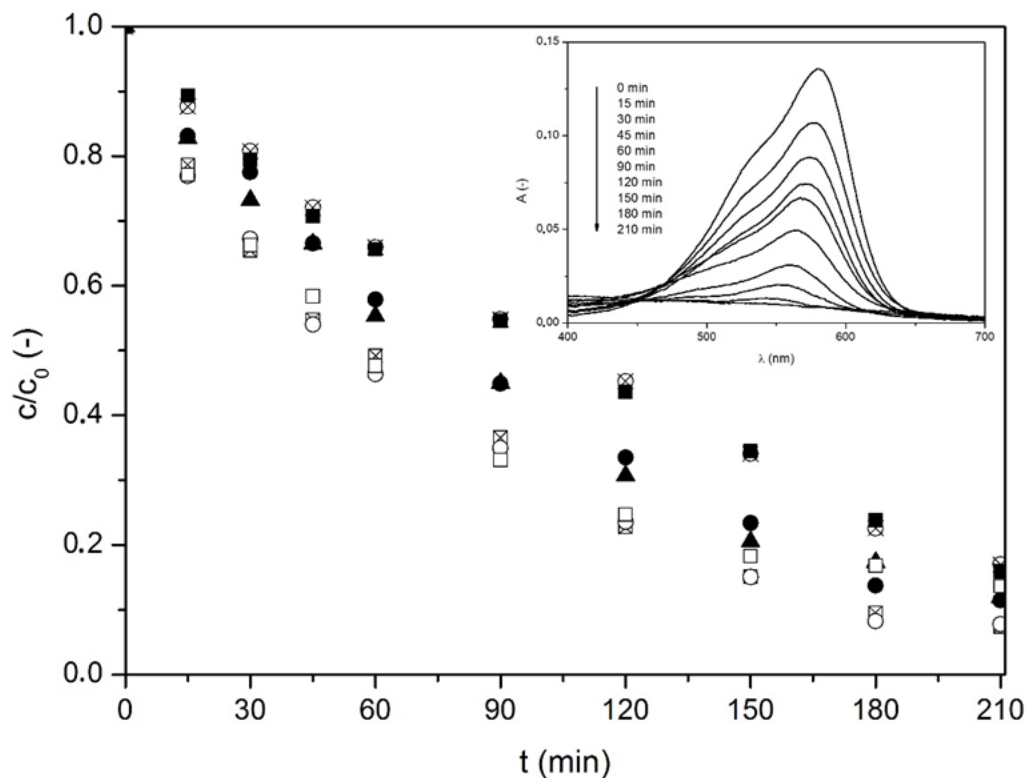

Figure 20 Photocatalytic degradation efficiency of Methyl Violet 2B by samples prepared in microwaves (MW11-16) and muffle furnace (MF) under UV light irradiation

CONCLUSIONS

The purpose of the presented dissertation was to develop and study new material systems with photocatalytic activity not only under UV light but also extend their photocatalytic activity to the visible light region. Moreover, governing factors and possibilities of further enhancement of photocatalytic performance of studied materials were investigated as an indispensable step prior their eventual application in surface modification of polymer and composite materials.

$$*****$$

A series of nanostructured ZnO micro-beads with mesoporous architecture was prepared to understand fundamental relationships between material properties of studied photocatalysts and their performance. The materials were prepared by annealing from a zinc oxalate dihydrate precursor at four different temperatures in an air atmosphere. X-ray diffraction data provided a set of structural and morphological parameters that were confirmed by SEM. Exemplary dependences of the specific surface area, the grain and crystallite volume, their ratio, pore length and diameter, and many other parameters were obtained. The interpretation allowed for finding crucial parameters governing the process at investigated hierarchical morphology and size scale levels. Let the factors promoting the photocatalytic activity be denoted by a (+) sign and impeding factors by a (-) sign. There are various size scales associated with the corresponding hierarchical levels [36]:

1. The size of the micro-lumps is in micrometres; however, their mesoporous morphology involves not only the length of the pores (macroscopic) but also their diameter (nm range) as representative physical length scales. Although the (BET) specific surface area (+) decreases monotonously, its availability for a photocatalytic reaction is controlled by geometrical constraints. The general pores flow geometric factor (+) decreases, while porosity (+) increases with the annealing temperature of micro-lumps preparation; hence, these trends work against each other.

2. The ZnO lumps are assembled from grains with a size scale mainly in hundreds of nanometers. The effect of the particle size (-) is manifested for particles bigger than the escape length of the exciton (actually its diffusion length) which is about 110 nm in ZnO. Both scattering or trapping of an exciton on an internal interface between nanocrystallites aggregated into the grain discriminates the exciton from the photocatalytic process. This effect increases with increasing grain size as illustrated by the decrease in both the packing factor (+) and the fraction of crystallites in the outer grain shell (+) with the annealing temperature of micro-lumps preparation.

3. At the level of the individual nanocrystallites, the size varies from ca 20 to 80 nm with applied annealing temperature. At this particle diameter length scale, the exciton radiation recombination rate (-) increases with the particle size, while intrinsic nanoparticle absorption (+) has a maximum of about 40 nm.

4. At the molecular level, the dominant role of holes in the photodegradation mechanism was revealed. They act mostly as agents directly oxidizing dye molecules adsorbed on the surface of the photocatalyst. Their role as producers of ROS is of minor importance. The effect of excited electrons as reducing agents triggering the superoxide radical pathway was revealed to be of the lowest importance.

*****

The basic ZnO studied in the first part of the work served as a reference and source material for further synthesis and investigation of extension of absorption edge of the traditional UV-light active ZnO photocatalyst towards visible-light in order to harvest the sunlight much more effectively. A simple method for the preparation of raspberry-like ZnO nanocrystals assembly with tunable optical properties, suitable for scaling-up was proposed. Modified samples outperformed the reference powder under visible light irradiation; thus, their photocatalytic activity has been shifted to the visible light region. Among other factors, the photocatalytic performance correlated at best yet moderately with the oxygen vacancy concentration in the material. Calcining of ZnO_2 precursor powder was shown to be an efficient route for introducing oxygen vacancies. The number of oxygen vacancies can be optimized by calcining temperature. However; their number increases with temperature, reaching maxima at ca 300 or 500 °C and then decreases, so the sample containing an optimum concentration of oxygen vacancies can be easily prepared by the control of calcining temperature and time.

Besides the study of these materials, a novel method intended for online measurement of visible light photocatalytic activity was developed. This method is advantageous over the commonly used experimental setups. It is based on the use of a homemade cuvette holder housing equipped with an LED mounted directly inside the UV-Vis spectrometer.

*****

Synthesis of a hybrid photocatalyst by coupling semiconductive ZnO and metallic Ag for enhancement of photocatalytic activity was successfully performed. Rapid, microwave-assisted hydrothermal method was used for the preparation of hierarchical ZnO and Ag/ZnO precursors with flower-like morphologies by using zinc acetate, silver nitrate, tripotassium citrate, and hexamethylenetetramine. The varying concentration of hydroxyl and citrate anions in the solution during the synthesis determines the resulting Zn- ligand,

and balance among them and play a crucial role in the formation mechanism of precursor morphology. While at lower pH, zinc citrate complexes sphere-like aggregates predominate, layered basic zinc acetate with flower-like morphology growth (appeared forms) via (following) dissolution- recrystallization mechanism when pH increases due to slow-release oh hydroxyl anions into the solution when hexamethylenetetramine decompose. Citrate anions, which plays a vital role in the formation mechanism of LBZA precursor, were used with advance to act simultaneously as a chelating and reducing agent for silver (Ag^+) cations. Flower-like LBZA precursor morphology decorated with Ag nanoparticles distributed uniformly onto its surface can be easily obtained by introducing silver nitrate into the reaction mixture. Nanostructured ZnO and Ag/ZnO morphologies possess flower-like shape after calcining of precursor materials at 500 °C. [39] The photocatalytic activities of samples were evaluated by photodegradation of MV2B under UV illumination. ZnO exhibits already an excellent photocatalytic activity due to the highly crystalline nanostructures which reduce charge carrier recombination probability because of shortening the pathway of photogenerated charged carriers, lowering the density of crystals defects, and stability of microstructured flowers against aggregation. Nevertheless, a significant improvement of photocatalytic activity was achieved by the decoration of the ZnO surface by Ag nanoparticles.

Use of hole and radical scavengers in the photodegradation study allowed elucidating the role of active species in the photocatalytic process occurring in studied hybride Ag/ZnO system. In this case, the direct oxidation of the dye molecule adsorbed on the surface by the hole is also the dominant mechanism. The secondary production of ROS by oxidation of OH^- is of moderate importance. Transfer of excited electrons from ZnO to the metallic silver nanoparticle greatly enhances charge separation and reduces futile exciton recombinations in the hybrid photocatalyst particles. As a result, the significant enhancement of the degradation rate constant was experienced due to increased availability of holes for oxidation. The minor mechanism of ROS generation by oxidation of OH^- was accelerated most likely as well. However, enhancement of the superoxide radical pathway of the degradation mechanisms was observed too, which can be explained by the increased availability of reducing electrons through silver nanoparticles.

*****

Although graphitic carbon nitride (g-C_3N_4) belongs to the most studied organic macromolecular photocatalyst nowadays, a new synthetic route and investigation of photocatalytic performance of this material yielded original results. The methodology for green synthesis of expanded g-C_3N_4 via rapid microwave-assisted heating of urea was successfully demonstrated. In contrast to the time consuming traditional synthesis methods in Muffle furnace, synthesis time can be

shortened to several minutes by direct utilization of microwaves. However, this requires the ability of the reaction mixture to absorb microwave radiation, which is not the case of urea used as a source compound. In principle, the use of a ceramic kiln placed into an MW oven cavity is a technique accelerating the synthesis even in comparison with the other type of MW synthesis using MW absorbing media. The kiln is lined with absorbing layer, which is heated up to glowing, and thus the energy is delivered into the reaction crucible in the form of heat radiation. Based on successful experience, the presented approach was proposed an alternative, which is generally applicable on variety of starting precursors, either single or mixtures. The microwaves assisted synthesis significantly affects the morphology of prepared g-C_3N_4 powders. The sample prepared traditionally in a muffle furnace exhibit morphology of small flakes with diameter around 1-2 μm, whereas powders obtained with assistance of MW in ceramic kiln are formed by expanded g-C_3N_4 aggregates with a diameter of around 20 μm. Optical properties can be finely tuned, covering the blue to green light region of visible light by varying the reaction conditions. Photocatalytic experiments revealed that adsorption capacity of prepared materials increases with increasing sample processing time, while the rate constant of photocatalytic degradation decreases. It can be ascribed to the expansion of the internal surface which results in worse availability of active sites to the diffusion transport of the dye. The removal of photodegradation products can also be impeded in this way. [38]

<center>*****</center>

Although the main body of the work was oriented on material tailoring of semiconductive metal oxide particular materials, the fourth studied system is a metal-free macromolecule with covalent bonds. All studied systems can be potentially used for the functionalization of surfaces of polymer articles. However, there is a plan in our group that such an extension of the work will invoke another dissertation and require a new doctoral student.

CLOSING REMARKS

Contribution to science and practice

For more than one century, heterogeneous semiconductor photocatalysis has received great scientific interest because of its application potential in diverse industrial sectors. Besides continuous scientific work on the water splitting, which historically constitutes a driving force in the research field of photocatalysis, many applications based on photocatalytic processes, such as self-cleaning, super-hydrophilic, anti-fogging, or antimicrobial surfaces already reach the mature market. Traditional photocatalysts possess wide band gaps, which means that they

can be activated only upon irradiation with photons of the wavelength of around 390-380 nm and lower. As the UV light account only of about 5 % of solar spectrum whereas visible light region approximately 40 %, search for visible-light responsive photocatalysts, which opens possibilities to employ solar light effectively is, together with never-ending efforts on increase of the overall efficiency of photocatalytic process a Holy Grail for researchers and material scientists all over the world.

This work represents a modest yet original contribution to the above described wide field of studies of semiconductor photocatalysis. **(i)** Since the most used photocatalysts are semiconductors effective only under UV irradiation due to a large width of their band-gaps, various types of ZnO photocatalysts were synthesized and characterized in terms of structure, properties, and photocatalytic activity during the first part of work on this thesis. **(ii)** Later, these photocatalysts were self-doped by native oxygen vacancies, and the effectivity of photocatalytic reaction was successfully shifted to the visible light region. **(iii)** In the third part of the thesis, the effect of decoration of photocatalysts by noble metal nanoparticles on the resulting photocatalytic activities under UV light irradiation was examined. The overall efficiency of the photocatalytic process was increased significantly. **(iv)** Lastly, an exemplary macromolecular organic photocatalyst (g-C_3N_4) was investigated, and its photocatalytic activity was also studied. **(v)** As a methodological contribution of the work, the simultaneously developed online system for measuring the photocatalytic activity by contemporary ISO standards can be considered.

Ongoing research and future prospective

The research in the field of photocatalytic materials does not stop with the accomplishment of the aim of this Thesis. The research Group of Multifunctional nanomaterials continues in the research of materials suitable for enhancement of the efficiency of photocatalytic processes under visible light. The work is oriented on the understanding structure-morphology-property-function relationship, thus aiming namely at the controlled design and synthesis of the materials with tailored performance. These particular materials are intended as building blocks for surface functionalization of polymer and composite articles with strong potential in large-area applications, e.g. in building façade constructions for cleaner cities and better living through material innovation in civil engineering.

Concerning the specific achievements presented in this Thesis, the future research and development will be focused both on the more detailed studies of the powder materials as well as on the issue of their applicability on polymer article surfaces intended for external conditions.

References

[1] G. Ciamician, THE PHOTOCHEMISTRY OF THE FUTURE, Science. 36 (1912) 385-394. doi:10.1126/science.36.926.385.

[2] K. Hashimoto, H. Irie, A. Fujishima, TiO2 photocatalysis: A historical overview and future prospects, Jpn. J. Appl. Phys. Part 1 - Regul. Pap. Brief Commun. Rev. Pap. 44 (2005) 8269-8285. doi:10.1143/JJAP.44.8269.

[3] N. Serpone, A.V. Emeline, S. Horikoshi, V.N. Kuznetsov, V.K. Ryabchuk, On the genesis of heterogeneous photocatalysis: a brief historical perspective in the period 1910 to the mid-1980s, Photochem. Photobiol. Sci. 11 (2012) 1121-1150. doi:10.1039/c2pp25026h.

[4] A. FUJISHIMA, K. HONDA, Electrochemical Photolysis of Water at a Semiconductor Electrode, Nature. 238 (1972) 3-+. doi:10.1038/238037a0.

[5] A. Fujishima, X. Zhang, D.A. Tryk, TiO2 photocatalysis and related surface phenomena, Surface Science Reports. 63 (2008) 515-582. doi://dx.doi.org/10.1016/j.surfrep.2008.10.001.

[6] A. Mills, S.K. Lee, A web-based overview of semiconductor photochemistry-based current commercial applications, J. Photochem. Photobiol. A-Chem. 152 (2002) 233-247. doi:10.1016/S1010-6030(02)00243-5.

[7] M.D. Hernandez-Alonso, F. Fresno, S. Suarez, J.M. Coronado, Development of alternative photocatalysts to TiO2: Challenges and opportunities, Energy Environ. Sci. 2 (2009) 1231-1257. doi:10.1039/b907933e.

[8] D. Spasiano, R. Marotta, S. Malato, P. Fernandez-Ibanez, I. Di Somma, Solar photocatalysis: Materials, reactors, some commercial, and pre-industrialized applications. A comprehensive approach, Appl. Catal. B-Environ. 170 (2015) 90-123. doi:10.1016/j.apcatb.2014.12.050.

[9] H. Tong, S. Ouyang, Y. Bi, N. Umezawa, M. Oshikiri, J. Ye, Nano-photocatalytic Materials: Possibilities and Challenges, Adv Mater. 24 (2012) 229-251. doi:10.1002/adma.201102752.

[10] M. Pelaez, N.T. Nolan, S.C. Pillai, M.K. Seery, P. Falaras, A.G. Kontos, P.S.M. Dunlop, J.W.J. Hamilton, J.A. Byrne, K. O'Shea, M.H. Entezari, D.D. Dionysiou, A review on the visible light active titanium dioxide photocatalysts for environmental applications, Appl. Catal. B-Environ. 125 (2012) 331-349. doi:10.1016/j.apcatb.2012.05.036.

[11] S.G. Ullattil, S.B. Narendranath, S.C. Pillai, P. Periyat, Black TiO2 Nanomaterials: A Review of Recent Advances, Chem. Eng. J. 343 (2018) 708-736. doi:10.1016/j.cej.2018.01.069.

[12] M.R. HOFFMANN, S.T. MARTIN, W.Y. CHOI, D.W. BAHNEMANN, Environmental Applications of Semiconductor Photocatalysis, Chem. Rev. 95 (1995) 69-96. doi:10.1021/cr00033a004.

[13] A. Mills, N. Wells, Reductive photocatalysis and smart inks, Chem. Soc. Rev. 44 (2015) 2849-2864. doi:10.1039/c4cs00279b.

[14] Y. Nosaka, A.Y. Nosaka, Generation and Detection of Reactive Oxygen Species in Photocatalysis, Chem. Rev. 117 (2017) 11302-11336. doi:10.1021/acs.chemrev.7b00161.

[15] T.A. Doane, A survey of photogeochemistry, Geochem. Trans. 18 (2017) 1. doi:10.1186/s12932-017-0039-y.

[16] Y. Zheng, C. Chen, Y. Zhan, X. Lin, Q. Zheng, K. Wei, J. Zhu, Y. Zhu, Luminescence and photocatalytic activity of ZnO nanocrystals: Correlation between structure and property, Inorg. Chem. 46 (2007) 6675-6682. doi:10.1021/ic062394m.

[17] A. Mclaren, T. Valdes-Solis, G. Li, S.C. Tsang, Shape and Size Effects of ZnO Nanocrystals on Photocatalytic Activity, J. Am. Chem. Soc. 131 (2009) 1254-+. doi:10.1021/ja9052703.

[18] B. Liu, X. Zhao, C. Terashima, A. Fujishima, K. Nakata, Thermodynamic and kinetic analysis of heterogeneous photocatalysis for semiconductor systems, Phys. Chem. Chem. Phys. 16 (2014) 8751-8760. doi:10.1039/c3cp55317e.

[19] A.V. Emeline, V.K. Ryabchuk, N. Serpone, Dogmas and misconceptions in heterogeneous photocatalysis. Some enlightened reflections, J Phys Chem B. 109 (2005) 18515-18521. doi:10.1021/jp0523367.

[20] M. Samadi, M. Zirak, A. Naseri, E. Khorashadizade, A.Z. Moshfegh, Recent progress on doped ZnO nanostructures for visible-light photocatalysis, Thin Solid Films. 605 (2016) 2-19. doi:10.1016/j.tsf.2015.12.064.

[21] C. Chen, W. Ma, J. Zhao, Semiconductor-mediated photodegradation of pollutants under visible-light irradiation, Chem. Soc. Rev. 39 (2010) 4206-4219. doi:10.1039/b921692h.

[22] J. Wang, Z. Wang, B. Huang, Y. Ma, Y. Liu, X. Qin, X. Zhang, Y. Dai, Oxygen Vacancy Induced Band-Gap Narrowing and Enhanced Visible Light Photocatalytic Activity of ZnO, ACS Appl. Mater. Interfaces. 4 (2012) 4024-4030. doi:10.1021/am300835p.

[23] M.Y. Guo, A.M.C. Ng, F. Liu, A.B. Djurisic, W.K. Chan, H. Su, K.S. Wong, Effect of Native Defects on Photocatalytic Properties of ZnO, J. Phys. Chem. C. 115 (2011) 11095-11101. doi:10.1021/jp200926uv.

[24] A.B. Djurisic, Y.H. Leung, A.M.C. Ng, Strategies for improving the efficiency of semiconductor metal oxide photocatalysis, Mater. Horizons. 1 (2014) 400-410. doi:10.1039/c4mh00031e.

[25] S.R. Forrest, M.E. Thompson, Introduction: Organic electronics and optoelectronics, Chem. Rev. 107 (2007) 923-925. doi:10.1021/cr0501590.

[26] Y.S. Zhao, H. Fu, A. Peng, Y. Ma, Q. Liao, J. Yao, Construction and Optoelectronic Properties of Organic One-Dimensional Nanostructures, Acc. Chem. Res. 43 (2010) 409-418. doi:10.1021/ar900219n.

[27] Z. Xie, C. Wang, K.E. deKrafft, W. Lin, Highly Stable and Porous Cross-Linked Polymers for Efficient Photocatalysis, J. Am. Chem. Soc. 133 (2011) 2056-2059. doi:10.1021/ja109166b.

[28] A. Naseri, M. Samadi, A. Pourjavadi, A.Z. Moshfegh, S. Ramakrishna, Graphitic carbon nitride (g-C3N4)-based photocatalysts for solar hydrogen generation: recent advances and future development directions, J. Mater. Chem. A. 5 (2017) 23406-23433. doi:10.1039/c7ta05131j.

[29] B. Mortazavi, G. Cuniberti, T. Rabczuk, Mechanical properties and thermal conductivity of graphitic carbon nitride: A molecular dynamics study, Comput. Mater. Sci. 99 (2015) 285-289. doi:10.1016/j.commatsci.2014.12.036.

[30] S. Cao, J. Low, J. Yu, M. Jaroniec, Polymeric Photocatalysts Based on Graphitic Carbon Nitride, Adv Mater. 27 (2015) 2150-2176. doi:10.1002/adma.201500033.

[31] U.I. Gaya, A.H. Abdullah, Heterogeneous photocatalytic degradation of organic contaminants over titanium dioxide: A review of fundamentals, progress and problems, J. Photochem. Photobiol. C-Photochem. Rev. 9 (2008) 1-12. doi:10.1016/j.jphotochemrev.2007.12.003.

[32] B. Bayarri, E. Carbonell, J. Gimenez, S. Esplugas, H. Garcia, Higher intrinsic photocatalytic efficiency of 2,4,6-triphenylpyrylium-based photocatalysts compared to TiO2P-25 for the degradation of 2,4-dichlorophenol using solar simulated light, Chemosphere. 72 (2008) 67-74. doi:10.1016/j.chemosphere.2008.01.075.

[33] J.C. Zhao, C.C. Chen, W.H. Ma, Photocatalytic degradation of organic pollutants under visible light irradiation, Top. Catal. 35 (2005) 269-278. doi:10.1007/s11244-005-3834-0.

[34] A. Mills, C. Hill, P.K.J. Robertson, Overview of the current ISO tests for photocatalytic materials, J. Photochem. Photobiol. A. 237 (2012) 7-23. doi://dx.doi.org/10.1016/j.jphotochem.2012.02.024.

[35] Sedlák, Jakub,, Univerzita Tomáše Bati ve Zlíně.,Technologická fakulta., Multiscale hierarchical ZnO-based composite systems = Víceměřítkové hierarchické kompozitní systémy na bázi ZnO : doctoral thesis summary, (2014).

[36] J. Sedlak, I. Kuritka, M. Masar, M. Machovsky, P. Janota, M. Dvorackova, P. Bazant, Contributions of morphological and structural parameters at different hierarchical morphology levels to photocatalytic activity of mesoporous nanostructured ZnO. Submitted under major revision, Applied Surface Science. (2019).

[37] M. Machovsky, I. Kuřitka, P. Saha, Rapid Microwave-Assisted Synthesis of Twinned Hexagonal ZnO Microparticles, , 2011.

[38] M. Masar, P. Urbanek, D. Skoda, B. Hanulikova, Z. Kozakova, M. Machovsky, L. Munster, I. Kuritka, Preparation and characterization of expanded g-C3N4 via rapid microwave-assisted synthesis, Diamond and Related Materials. 83 (2018) 109-117. doi:10.1016/j.diamond.2018.01.028.

[39] L. Di, H. Yang, T. Xian, X. Chen, Enhanced Photocatalytic Degradation Activity of BiFeO3 Microspheres by Decoration with g-C3N4 Nanoparticles, Mater. Res. -Ibero-am. J. Mater. 21 (2018). doi:10.1590/1980-5373-MR-2018-0081.

List of figures

List of symbols, acronyms, and abbreviations

Besides ubiquitous terms and standard abbreviations (e.g., XRD) or standard nomenclature (ZnO), following symbols, acronyms, and abbreviations were used in this Thesis.

UV	Ultraviolet	L-H	Langmuir-Hinshelwood
ISO	International standards organization	Vis	Visible
ROS	Reactive oxygen species	CPS	Centre of Polymer Systems
IUPAC	The International Union of Pure and Applied Chemistry	FWHM	The full width at half maximum
		PL	Photoluminescence
VB	The valence band	MV2B	Methylene blue 2B
CB	The conduction band	LED	Light-Emitting Diode
A	Acceptor	QG	Quartz glass
D	Donor	LBZA	Layered basic zinc acetate
NHE	Normal hydrogen electrode	MW	Microwave
		MF	Muffle furnace

CURRICULUM VITAE

Personal information

First name(s) / Surname(s): Milan Masař

Address: 306, Řetechovská, 76326, Luhačovice, The Czech Republic

Date of birth: 01. 08. 1990

Telephone / Mobile: 736144533

E-mail: masar@ utb.cz

Nationality: Czech

Gender: Male

Education

Dates: 2015 – to date

Ph.D. studies in Chemistry and Materials Technology, Specialization: Technology of Macromolecular Compounds

Faculty of Technology - Tomas Bata University in Zlín

Dates: 2013 - 2015

Master's programme in Chemistry and Materials Technology, degree course in Medical and Pharmaceutical Materials

Faculty of Technology - Tomas Bata University in Zlín

Master's thesis topic: Preparation and Study of Photocatalytic Activity of Selected Semiconductor Materials

Dates: 2011 - 2013

Bachelor's programme in Chemistry and Materials Technology, degree course in Medical and Pharmaceutical Materials

Faculty of Technology - Tomas Bata University in Zlín

Bachelor's thesis topic: Preparation of ZnO Sub-micro and Nanostructures

Dates: 2006 - 2010

Name and type of organisation providing education and training: J. A. Komenský Grammar School Uherský Brod

Projects

IGA/CPS/2015/005 – Study of synthetic polymer and biopolymer blends – member of the research team

IGA/CPS/2016/006 – Synthesis of functional fillers on the basis of metal oxides and sulphides – project leader

IGA/CPS/2017/007 – Preparation and characterization of nanostructured polymeric and composite systems – a member of the research team/project leader

IGA/CPS/2018/007 – Development and studies of conductive nanocomposite systems applicable in polymer electronics – project leader

IGA/CPS/2019/007 – Development and study of conductive nanocomposite materials for electronic and electrotechnical applications – a member of the research team

NPU I LO1504 – Centre of Polymer Systems plus – research project worker

GA19-23531S; GA19-23647S; and CZ.02.2.69/0.0/0.0/16_028/0006243 – research project worker

Pedagogic activities

Participated in teaching in laboratory classes of "Preparation and Characterization Methods" and "Nanomaterials and Nanotechnology II."

Training

Summer school of electron microscopy – Institute of Scientific Instruments (Brno 2015)

Measurement of vibration spectra – University of Chemistry and Technology (Prague 2016)

Interpretation of vibration spectra – University of Chemistry and Technology (Prague 2016)

MiniFlex training (X-ray diffraction and PDXL analysis) – Rigaku (Germany 2016)

Internship - Politechnika Rzeszowska - Erasmus+ (Poland 2019)

List of publications

1. MASAR, M., URBANEK, P., SKODA, D., HANULIKOVA, B., KOZAKOVA, Z., MACHOVSKY, M., MUNSTER, L. and KURITKA, I. Preparation and characterization of expanded g-C3N4 via rapid microwave-assisted synthesis. *Diamond and Related Materials* **83**, 109-117 (2018).

2. MASAR, M., URBANEK, M., URBANEK, P., MACHOVSKA, Z., MASLIK, J., YADAV, R. S., SKODA, D., MACHOVSKY, M. and KURITKA, I. Synthesis, characterization and examination of photocatalytic performance of hexagonal covellite CuS nanoplates. *Materials Chemistry and Physics* **237**, 121823 (2019).

3. YADAV, R. S., KURITKA, I., VILCAKOVA, J., HAVLICA, J., KALINA, L., URBÁNEK, P., MACHOVSKY, M., MASAR, M. and HOLEK, M. Influence of La3+ on structural, magnetic, dielectric, electrical and modulus spectroscopic characteristics of single phase CoFe2-xLaxO4 nanoparticles. *Journal of Materials Science-Materials in Electronics* **28**, 9139-9154 (2017).

4. MÜNSTER, L., VÍCHA, J., KLOFÁC, J., MASAR, M., KUCHARCZYK, P. and KURITKA, I. Stability and aging of solubilized dialdehyde cellulose. *Cellulose* **24**, 2753-2766 (2017).

5. YADAV, R. S., KURITKA, I., VILCAKOVA, J., URBÁNEK, P., MACHOVSKY, M., MASAR, M. and HOLEK, M. Structural, magnetic, optical, dielectric, electrical and modulus spectroscopic characteristics of ZnFe2O4 spinel ferrite nanoparticles synthesized via honey-mediated sol-gel combustion method. *Journal of Physics and Chemistry of Solids* **110**, 87-99 (2017).

6. YADAV, R. S., KURITKA, I., VILCAKOVA, J., HAVLICA, J., KALINA, L., URBÁNEK, P., MACHOVSKY, M., SKODA, D., MASAR, M. and HOLEK, M. Sonochemical synthesis of Gd3+ doped CoFe2O4 spinel ferrite nanoparticles and its physical properties. *Ultrason. Sonochem.* **40**, 773-783 (2018).

7. YADAV, R. S., KURITKA, I., VILCAKOVA, J., HAVLICA, J., KALINA, L., URBÁNEK, P., MACHOVSKY, M., SKODA, D. and MASAR, M. Influence of Gd3+-substitution on structural, magnetic, dielectric and modulus spectroscopic characteristics of ZnFe2O4 spinel ferrite nanoparticles. *Journal of Materials Science-Materials in Electronics* **29**, 15878-15893 (2018).

8. MASLIK, J., KURITKA, I., URBANEK, P., KRCMAR, P., SULY, P., MASAR, M. and MACHOVSKY, M. Water-Based Indium Tin Oxide Nanoparticle Ink for Printed Toluene Vapours Sensor Operating at Room Temperature. *Sensors* **18**, 3246 (2018).

9. MÜNSTER, L., VÍCHA, J., KLOFÁC, J., MASAR, M., HURAJOVÁ, A. and KURITKA, I. Dialdehyde cellulose crosslinked poly(vinyl alcohol) hydrogels: Influence of catalyst and crosslinker shelf life. *Carbohydr. Polym.* **198**, 181-190 (2018).

10. PLACHY, T., KUTALKOVA, E., SEDLACIK, M., VESEL, A., MASAR, M. and KURITKA, I. Impact of corrosion process of carbonyl iron particles on magnetorheological behavior of their suspensions. *Journal of Industrial and Engineering Chemistry* **66**, 362-369 (2018).

11. BAKAR, M., BIALKOWSKA, A., KURITKA, I., HANULIKOVÁ, B. and MASAR, M. Synergistic effects of thermoplastic and nanoclay on the performance properties and morphology of epoxy resin. *Polymer Composites* **39**, E2551 (2018).

12. PLACHY, T., MASAR, M., MRLIK, M., MACHOVSKY, M., MACHOVSKA, Z., KUTALKOVA, E. and KURITKA, I. Switching between negative and positive electrorheological effect of g-C3N4 by copper ions doping. *Advanced Powder Technology* **30**, 714-723 (2019).

13. YADAV, R. S., KURITKA, I., VILCÁKOVÁ, J., MACHOVSKÝ, M., ŠKODA, D., URBÁNEK, P., MASAR, M., GORALIK, M., URBÁNEK, M., KALINA, L. and HAVLICA, J. Polypropylene Nanocomposite Filled with Spinel Ferrite NiFe2O4 Nanoparticles and In-Situ Thermally-Reduced Graphene Oxide for Electromagnetic Interference Shielding Application. *Nanomaterials* **9**, 621 (2019).

14. YADAV, R. S., KURITKA, I., VILCAKOVA, J., SKODA, D., URBÁNEK, P., MACHOVSKY, M., MASAR, M., KALINA, L. and HAVLICA, J. Lightweight NiFe2O4-Reduced Graphene Oxide-Elastomer Nanocomposite flexible sheet for electromagnetic interference shielding application. *Compos Part B: Eng* **166**, 95-111 (2019).

Overview of other activities

Conferences:

1. MACHOVSKY, M., MASAR, M., PASTOREK, M., URBANEK, P. and KURITKA, I. *Microwave-assisted solvothermal synthesis and characterization of nanostructured Cu2SnS3 architectures* (NANOCON 2015 - 7th International Conference on Nanomaterials - Research and Application, Conference Proceedings, 2015).

2. MASAR, M., MACHOVSKÝ, M., URBÁNEK, M., URBÁNEK, P., ANTOŠ, J. and KURITKA, I. *On-line measurement of photocatalytic activity of powdered samples* (NANOCON 2016 - Conference Proceedings, 8th International Conference on Nanomaterials - Research and Application, 2016).

3. MASAR, M., MACHOVSKÝ, M., URBÁNEK, P., URBÁNEK, M. and KURITKA, I. *Biotemplated synthesis of nanostructured ZnO with enhanced visible light photocatalytic activity* (NANOCON 2017 - Conference Proceedings,

9th International Conference on Nanomaterials - Research and Application Ser. 2017-October, 2018).

4. PEER, P., POLÁSKOVÁ, M., MOSNÁCEK, J., SEDLARIKOVÁ, J. and MASAR, M. *Preparation and characterization of fibrous non-woven textile decorated by silver nanoparticles for water filtration* (NANOCON 2018 - Conference Proceedings, 10th Anniversary International Conference on Nanomaterials - Research and Application, 2019).

5. JURCA, M., GORALIK, M., VILCAKOVA, J., KAZANTSEVA, N., MASAR, M., and FOULGE, S. Enhanced electrical conductivity of immiscible blends filled with nickel particles. *Abstr. Pap. Am. Chem. Soc.* **257** (2019)

Milan Masař

Příprava a charakterizace funkčních plniv s fotokatalytickou aktivitou

Preparation and characterization of nanomaterials with photocatalytic activity

Doctoral Thesis Summary